

CERN 82-13
Super Proton-Synchrotron
Division
23 December 1982

ORGANISATION EUROPÉENNE POUR LA RECHERCHE NUCLÉAIRE
CERN EUROPEAN ORGANIZATION FOR NUCLEAR RESEARCH

THE CEDAR COUNTERS FOR PARTICLE IDENTIFICATION
IN THE SPS SECONDARY BEAMS:
A DESCRIPTION AND AN OPERATION MANUAL

C. Bovet, R. Maleyran, L. Piemontese,
A. Placci and M. Placidi

GENEVA
1982

© Copyright CERN, Genève, 1982

Propriété littéraire et scientifique réservée pour tous les pays du monde. Ce document ne peut être reproduit ou traduit en tout ou en partie sans l'autorisation écrite du Directeur général du CERN, titulaire du droit d'auteur. Dans les cas appropriés, et s'il s'agit d'utiliser le document à des fins non commerciales, cette autorisation sera volontiers accordée.

Le CERN ne revendique pas la propriété des inventions brevetables et dessins ou modèles susceptibles de dépôt qui pourraient être décrits dans le présent document; ceux-ci peuvent être librement utilisés par les instituts de recherche, les industriels et autres intéressés. Cependant, le CERN se réserve le droit de s'opposer à toute revendication qu'un usager pourrait faire de la propriété scientifique ou industrielle de toute invention et tout dessin ou modèle décrits dans le présent document.

Literary and scientific copyrights reserved in all countries of the world. This report, or any part of it, may not be reprinted or translated without written permission of the copyright holder, the Director-General of CERN. However, permission will be freely granted for appropriate non-commercial use. If any patentable invention or registrable design is described in the report, CERN makes no claim to property rights in it but offers it for the free use of research institutions, manufacturers and others. CERN, however, may oppose any attempt by a user to claim any proprietary or patent rights in such inventions or designs as may be described in the present document.

CERN - Service d'Information scientifique - RD/571 - 1200 - janvier 1983

ABSTRACT

The Čerenkov Differential counter with Achromatic Ring Focus (CEDAR) has been designed and a number built at CERN for the identification (and selection) of particles in the secondary beams of a high-energy accelerator. CEDAR-N can separate kaons from pions up to 300 GeV/c but can detect protons only down to 60 GeV/c; **CEDAR-W can flag protons of 12 GeV/c and separate kaons from pions up to 150 GeV/c.** After a brief account of the relevant physics of the Čerenkov effect, this report describes CEDARs with emphasis on those characteristics and construction features that are of interest to the user. Details are given of the high-precision optical system, the mechanical construction to achieve uniform temperature (0.1 K) and rigidity, and the gas handling and measurement. The layout of the CEDARs in the secondary beams of the CERN Super Proton Synchrotron is described. The signals provided to the user are listed and explained, together with the programs for on-line control of the counters. Details are given of the performances attained, together with various hints and suggestions on the procedure to follow in order to set-up, tune, and operate a CEDAR. The dependence of the performance on beam optics is stressed.

CONTENTS

	Page
1. INTRODUCTION	1
2. PRINCIPLE OF OPERATION AND OPTICAL RESOLUTION	2
2.1 Principle of operation	2
2.2 Effects broadening the light spot	4
2.3 Choice of parameters	6
2.4 Pattern recognition	8
2.5 Efficiency and rejection	8
3. DESCRIPTION OF CEDAR COUNTERS	9
3.1 Optical system	9
3.1.1 Chromatic corrector	9
3.1.2 Mangin mirror	11
3.1.3 Optical tests	12
3.1.4 Light output	13
3.2 Mechanical engineering	14
3.2.1 Temperature uniformity	14
3.2.2 Windows	14
3.2.3 Optical tower	14
3.2.4 Ring diaphragm	14
3.2.5 Alignment table	15
3.3 Gas controls	15
3.3.1 Measurement of the index of refraction	16
3.3.2 Gas pressure monitoring and absolute calibration	17
3.3.3 Gas handling	17
4. LAYOUT, ELECTRONICS, AND COMPUTER CONTROLS	18
4.1 Layout	18
4.2 Electronics for signal treatment	18
4.3 Computer controls	20
5. PRACTICAL OPERATION	25
5.1 Particle separation and CEDAR resolution	26
5.2 Efficiency	27
5.3 Procedure for the tuning and setting up of a CEDAR	28
5.4 Monitoring the CEDAR stability	30
5.5 Operation at high beam intensity	30
5.6 Selection of electrons and muons	30

	Page
APPENDIX A: STATISTICS OF PATTERN RECOGNITION	33
APPENDIX B: ALGORITHM FOR COMPUTER CONTROL OF THE INDEX OF REFRACTION	35
APPENDIX C: GENERAL MECHANICAL DRAWING	37

1. INTRODUCTION

The CERN Super Proton Synchrotron (SPS) secondary beams have been instrumented with a set of various detectors, including analog wire chambers for measurement of beam-spot position and size, scintillator-filament scanners to optimize the beam divergence, MultiWire Proportional Counters (MWPCs) for measurement of the momentum of individual particles, and Čerenkov counters for particle identification.

The latter include threshold Čerenkov counters for applications at lower energies, and counters of the Differential Isochronous Self-collimating Čerenkov (DISC) type for better resolution mainly at higher energies. A variety of these differential counters, called Čerenkov Differential counters with Achromatic Ring focus (CEDARs), have been designed and built in the SPS Division as an experimental facility: 13 CEDARs are now operational and have been successfully used in the North or West Area beams (see the example of Fig. 1).

Two types of CEDAR exist: the CEDAR-N and the CEDAR-W, with obvious reference to the North and West experimental areas. They differ in the energy range to which they are adapted: the CEDAR-N can separate K's from π 's up to 300 GeV/c, but can detect protons only down to about 60 GeV/c, while the CEDAR-W can flag protons of 12 GeV/c, and can separate K's from π 's up to about 150 GeV/c. The CEDAR's electronics is also provided and serviced by the SPS Experimental Area (EA) Group. The CEDAR's commands and the electronics are under computer

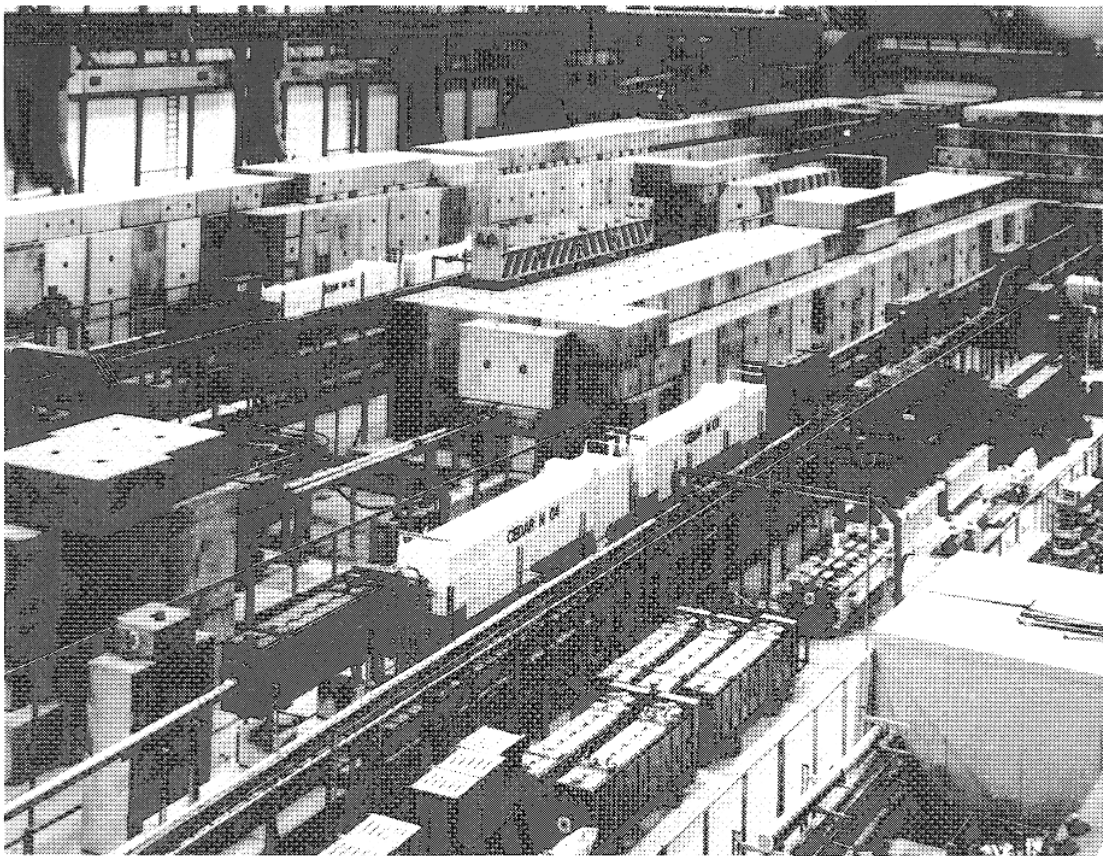


Fig. 1 CEDAR counters installed in a secondary beam line

control, and are connected to the SPS computer network. The user receives the CEDAR's signals and can operate his CEDAR as well as tune his magnets and collimators from a keyboard in his counting room.

Despite all the facilities available, it is a delicate enterprise to tune and optimize a CEDAR and to keep it in the best condition during data taking. Users have to learn how to set it properly, how to check it, and how to find the reason for a malfunctioning.

In Section 2 the principles of operation and the optical resolution of a CEDAR are described, and the fundamental limitations of the instrument are emphasized. In Section 3 details of and comments on all relevant parameters of the counters are given. In Section 4 the environment of the CEDARs in a beam line and the electronic treatment of the signals are explained, and a thorough description of the software available for interactive controls and diagnostics is given. Finally, in Section 5, rules for practical operation are given and a complete procedure for tuning and setting up a CEDAR is presented.

The main scope of the present report is to help the user to better understand the instrument with a view to assessing its possible performances, to finding the optimum tuning for efficiency and rejection, and to running and monitoring the CEDAR during all data taking.

2. PRINCIPLE OF OPERATION AND OPTICAL RESOLUTION

2.1 Principle of operation

The Čerenkov light produced by a beam particle is emitted on cones of semi-aperture θ with

$$\cos \theta = \frac{1}{n\beta} , \quad (1)$$

where n is the index of refraction of the transparent medium and β is the velocity of the particle.

Differential counters have an optical system to focus this light to give a ring image (see Fig. 2), with the aim of distinguishing particles with different masses according to the diameter of the light rings.

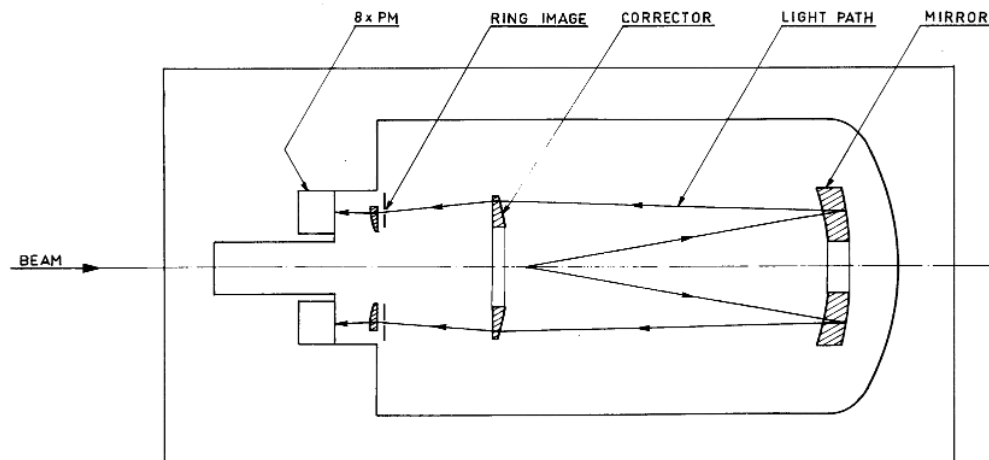


Fig. 2 Schematics of the optics of a differential Čerenkov counter (distorted scale)

The velocity of a particle is given by

$$\beta = \left[1 + \left(\frac{m}{p} \right)^2 \right]^{-\frac{1}{2}}, \quad (2)$$

where m and p are its mass and momentum, and $c = 1$. It is clear from Eq. (2) that the different momenta in a secondary beam with $\Delta p/p \approx 1\%$ do not play much role compared with mass differences of 100% or more. For two masses m_1 and m_2 one can write

$$\frac{\Delta\beta}{\beta} \approx \beta_2 - \beta_1 = \left[1 + \left(\frac{m_2}{p} \right)^2 \right]^{-\frac{1}{2}} - \left[1 + \left(\frac{m_1}{p} \right)^2 \right]^{-\frac{1}{2}} \approx \frac{m_2^2 - m_1^2}{2p^2}. \quad (3)$$

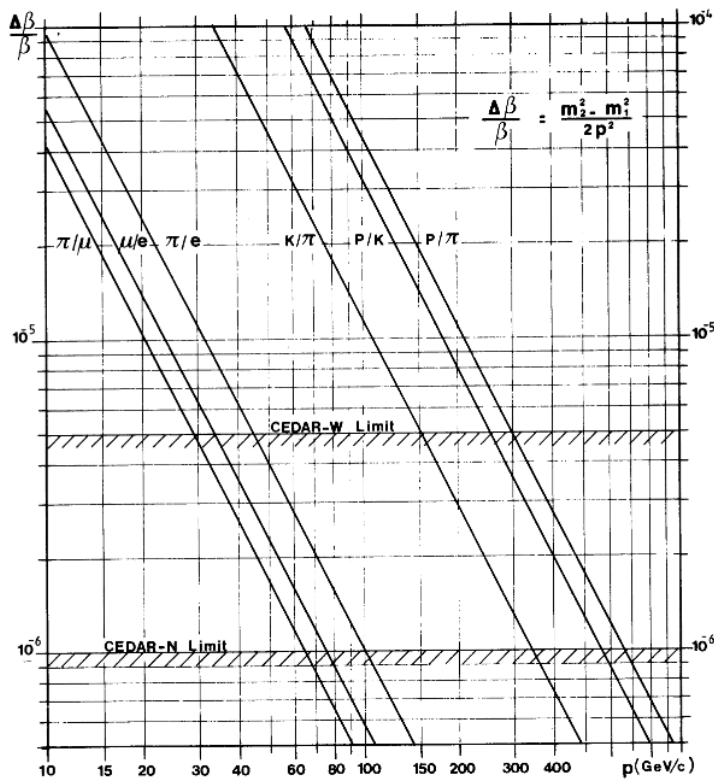


Fig. 3 Velocity difference $\Delta\beta/\beta$ vs. momentum

Figure 3 illustrates the differences of velocity $\Delta\beta/\beta$, corresponding to various pairs of particles with masses m_1 and m_2 , as a function of momentum.

Differentiating Eq. (1), with n constant, gives

$$\Delta\theta = \frac{1}{\tan\theta} \frac{\Delta\beta}{\beta} \approx \frac{1}{\theta} \frac{\Delta\beta}{\beta}, \quad (4)$$

and the difference in the ring radius R , which should allow separation of the particles, is given by

$$\Delta R = f \Delta\theta = \frac{f}{\theta} \frac{m_2^2 - m_1^2}{2p^2}, \quad (5)$$

where f is the focal length of the system. A mechanical diaphragm, with variable annular opening LD , is located in the focal plane to select the photons of the wanted particles. Rings can be distinguished if their radii differ by $\Delta R > LD$. In practice LD can be set as small as 0.1 ± 0.01 mm but it is a difficult optical problem to focus the light into such a sharp ring image.

2.2 Effects broadening the light spot

Various effects must be corrected for in order to minimize the width of the light rings:

- i) **Optical aberrations** such as astigmatism, coma, and spherical aberrations exist, of course, but have been minimized and contribute to only 20 μm FWHM in CEDAR optics. The diffraction limit for telescope optics with $f:15$ and $\lambda = 300$ nm is $d_{\min} = 6 \mu\text{m}$ and can be neglected.
- ii) The most severe effect is the **chromatic dispersion** which may be expressed as

$$\Delta R_{\text{ch}} = f\theta \frac{1}{2v} \left(1 + \frac{1}{\theta^2 \gamma^2} \right), \quad (6)$$

where $v = (n_D - 1)/(n_F - n_C)$ is the **Abbé number**, which characterizes the reciprocal dispersion of the gas ($\lambda_D = 589.3$ nm, $\lambda_F = 486.1$ nm, $\lambda_C = 656.3$ nm). v must be selected as large as possible and is one of the most important criteria in the choice of the gas. At high energy the term $1/\theta^2 \gamma^2$ in Eq. (6) can be neglected and the chromatic dispersion is directly proportional to θ , which must therefore be chosen as small as possible. In order to improve their resolution further DISC and CEDAR counters have an optical corrector to reduce the chromatic dispersion [see other papers¹⁻³⁾ and Section 3].

- iii) The **multiple scattering** incurred by the beam during its traversal of the gas radiator also contributes to broadening the light ring. Indeed the centre of the light ring is defined by the direction of the particle trajectory. If this direction changes inside the counter, the photons are spread around non-concentric circles, resulting in a broadening of the spot (see Fig. 4b). This effect is the most important one when the two previous effects have been corrected for, and therefore the radiation length is also a vital parameter to consider in the choice of the gas. The r.m.s. of the light distribution due to the gas scattering is

$$\sigma_{R(\text{sc})} = f \frac{15}{8p} \sqrt{\frac{LP}{3X_0}}, \quad (7)$$

where L is the length of the gas radiator, which has radiation length X_0 , and pressure P . The factor 3 under the square root of Eq. (7) comes from the averaging over the length of the radiator.

- iv) The **inhomogeneity of the index of refraction** of the radiator contributes to the width of the light rings as follows:

$$\Delta R = \frac{f}{\tan \theta} \frac{\Delta n}{n}, \quad (8)$$

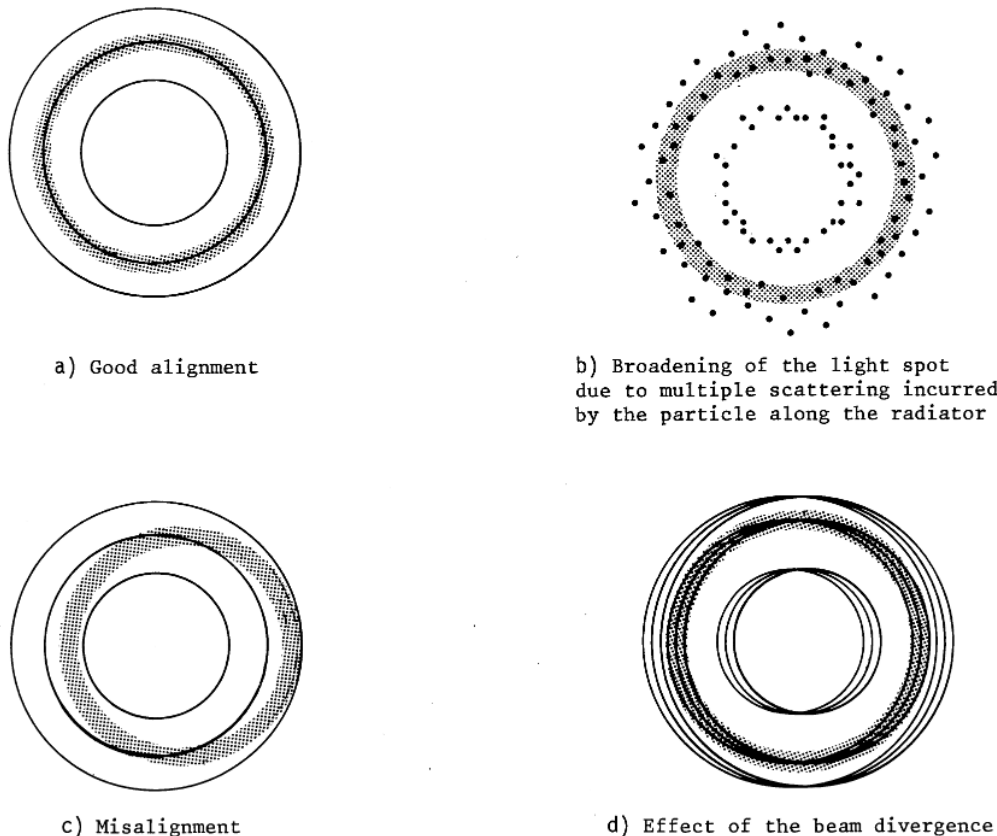


Fig. 4 Photon distribution in the plane of the diaphragm (the shaded areas represent the diaphragm opening)

as can be deduced from Eqs. (1) and (5), and from Eq. (4) where $\Delta n/n$ should replace $\Delta\beta/\beta$. In a CEDAR no pressure gradient exists in a steady condition, but a temperature distribution may persist for long periods of time (see Section 3). Let us assume a linear variation of temperature along the length L of the radiator, with a gradient $\Delta T/L$. Since $\Delta n/n$ is proportional to $\Delta T/T$ at constant pressure [Eq. (20), p. 16], the photons will have a rectangular distribution in R with a standard deviation

$$\sigma_{R(T)} = \frac{1}{2\sqrt{3}} \frac{1-n}{n} \frac{f}{\tan \theta} \frac{\Delta T}{T} . \quad (9)$$

These four effects are incoherent and contribute to limiting the resolution. The next effect is coherent for any given particle and results in a broadening of the light spot only when averaging is made over many particles.

- v) The beam divergence creates another problem, since the light rings are concentric only when the particles have parallel trajectories. If not the projected angles x' and y' of a particle trajectory result in a displacement of the centre of the light ring by amounts

$$\Delta x = fx' , \quad \Delta y = fy' . \quad (10)$$

Hence the light distribution averaged over many particles is characterized by

$$\begin{aligned}\sigma_R(x') &= f\sigma_x' \\ \sigma_R(y') &= f\sigma_y'\end{aligned}\quad (11)$$

as illustrated in Fig. 4d, where σ_x' and σ_y' correspond to the beam divergence.

Note that this effect is generally different in the horizontal and vertical planes; furthermore, it does not concern all particles to the same degree since those with small x' or y' are affected less than those with large x' or y' . In other words, a CEDAR has an efficiency which decreases with increasing angle between the particle trajectory and the optical axis (see Fig. 5, for a typical example, where the sixfold efficiency is shown and x' and y' are scaled in units of LD/f).

- vi) Other sources contribute to the background between the particle peaks, such as the photomultiplier noise, the light produced by halo particles hitting optical components, or the scintillation light produced by beam particles in the gas.

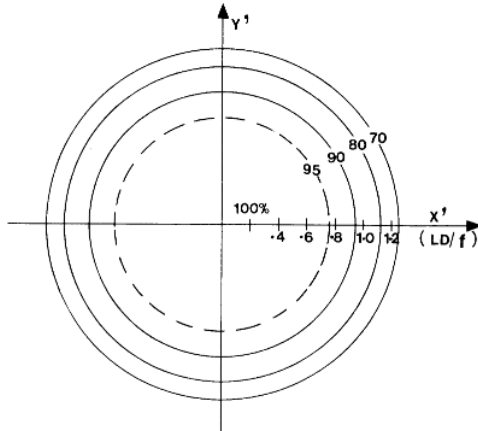


Fig. 5 CEDAR efficiency as a function of beam divergence

2.3 Choice of parameters

The choice of many parameters of the counter is the result of an overall optimization of performance made by a computer simulation of the light collection. We are not going to describe this procedure in detail but just want to recall the physical arguments which compete with one another.

The number of photons of Čerenkov light emitted is given by⁴⁾:

$$N_{ph} = 2\pi\alpha L \sin^2 \theta \int \frac{d\lambda}{\lambda^2}, \quad (12)$$

where α is the fine-structure constant, L the length of the radiator, and the integral extends to the range of wavelengths accepted by the system.

Thus three parameters influence the light output: the Čerenkov angle θ , the length of the radiator, and the width of the accepted spectrum especially towards small wavelengths.

radiator = gas

But in order to reach a good velocity resolution the counters need to have, according to Eq. (4),

$$\theta \Delta\theta \ll \frac{\Delta\beta}{\beta}, \quad (13)$$

Now the resolution in θ is merely defined by the chromatic dispersion of Eq. (6), which can be simplified to

$$\Delta\theta_{ch} = \frac{\theta}{2v}, \quad (14)$$

when the counter is used at high energy ($\gamma > 1/\theta$).

Combining Eqs. (13) and (14), we get

$$\frac{\theta^2}{2kv} \ll \frac{\Delta\beta}{\beta}, \quad (15)$$

where k is the correction factor achieved by the chromatic corrector, and one sees that, for optimal resolution, θ should be small in contradiction with the light output requirement. To reach a good value of k one also tends to reduce the spectral range which is detrimental to the light output; and the length of the radiator is limited for consideration of the beam layout in the experimental halls. The choice of the gases was made in order to minimize the chromatic dispersion (large v) and the multiple scattering, and with a view to the minimum momentum p_{min} which could be achieved within 15 bar (the maximum pressure at which the counter can be operated).

Table 1
Design parameters

CEDAR type	W	N
$\Delta\beta/\beta_{sep}$	5×10^{-6}	10^{-6}
Gas	N_2	He
$(n_0 - 1) \times 10^6$	292.0	38.7
v	35	54
θ (mrad)	30.9	25.8
k	11	24
$\theta^2/2kv$	1.2×10^{-6}	2.6×10^{-7}
L (m)	3.24	3.88
p_{min}/m	11.3	55.9

These considerations, together with the optical system which is described in Section 3, have led to the choice of the parameters given in Table 1. The lowest momenta at which the counters can be set to detect particles of mass m are given as a ratio p_{min}/m . Working pressure P and multiple scattering (θ)_{sc} resulting from a full traversal of the counter are illustrated in Figs. 6 and 7.

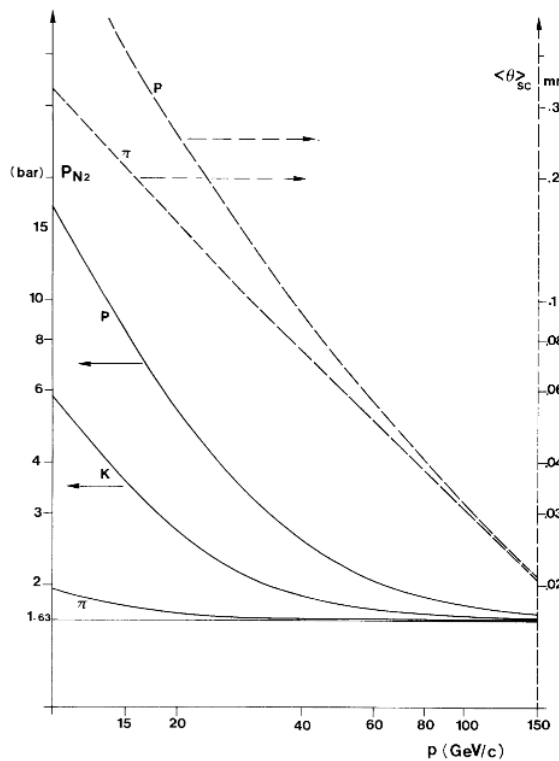


Fig. 6 Working pressure and multiple scattering for CEDAR-W (gas: N_2)

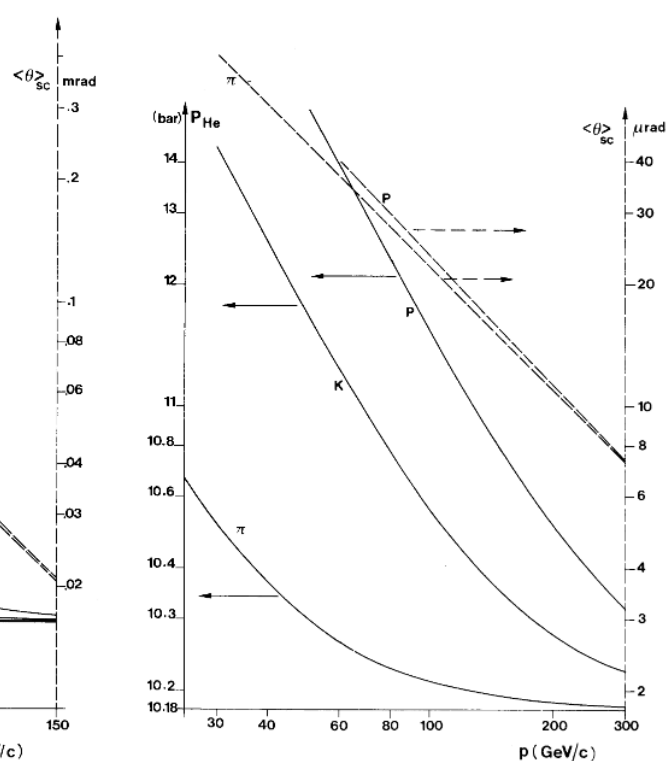


Fig. 7 Working pressure and multiple scattering for CEDAR-N (gas: He)

2.4 Pattern recognition

The main aim here is to discard the signal produced by unwanted particles, i.e. rings of a slightly different diameter. This is best done by collecting the light through a circular diaphragm of variable aperture, LD, and focusing it onto a number of photomultipliers. This number must be large enough to provide a good discrimination against wrong rings of light even when one or two photomultipliers are failing to detect the event. CEDAR counters have eight photomultipliers, so that the discrimination against unwanted particles is good when at least five photomultipliers give signals.

The detection of good particles must also have a sufficient immunity against random background as identified in Section 2.1, paragraph (vi). For that a high level of coincidence between the photomultiplier signals will also be the best ingredient. Signals with majority counts of eightfold, sevenfold and sixfold coincidence are provided for the user. The level of coincidence plays an important role in the relation of efficiency to rejection.

$$\text{coincidence} = ???$$

2.5 Efficiency and rejection

For a given photomultiplier the efficiency η of recording the signal is given by

$$\eta = 1 - e^{-\phi}, \quad (16)$$

where ϕ is the average number of recorded photoelectrons; see Appendix A.

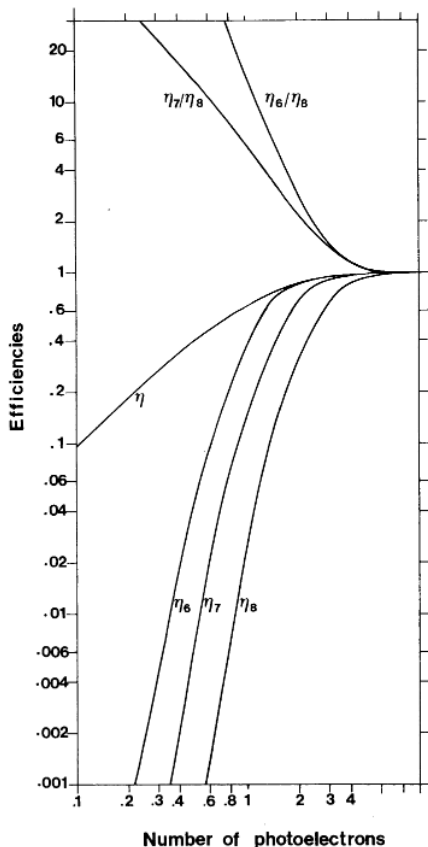


Fig. 8 Efficiency as a function of the average number of photoelectrons per photomultiplier

If eight photomultipliers are watching the same event with similar efficiencies η , then the probability of observing the different levels of coincidence -- eight, seven, and six -- is given by

$$\begin{aligned}\eta_8 &= (1 - e^{-\phi})^8 \\ \eta_7 &= \eta_8 + 8 (1 - e^{-\phi})^7 e^{-\phi} \\ \eta_6 &= \eta_7 + 28 (1 - e^{-\phi})^6 e^{-2\phi}.\end{aligned}\quad (17)$$

These values are shown in Fig. 8, where the number of photoelectrons, for a typical operation of a CEDAR, is in the range $1 < \phi < 4$.

In practice, ϕ can be determined experimentally, when the CEDAR is set correctly, by counting simultaneously the number of coincidences of various levels: N_6 , N_7 , N_8 . Since these numbers are in direct proportion to the efficiencies η_6 , η_7 , η_8 , their ratios can be substituted for the ratios η_7/η_8 in Eq. (A.8) and for η_6/η_8 in Eq. (A.11), and values of ϕ can be calculated.

These values are then used in their turn to compute the absolute efficiencies for sixfold, sevenfold and eightfold coincidence levels, through Eq. (17), and the information so obtained is vital for the user to check that the counter keeps in good running condition.

3. DESCRIPTION OF CEDAR COUNTERS

3.1 Optical system

The optical system of a CEDAR focuses most of the Čerenkov light onto the plane of the diaphragm with the help of a spherical mirror whose production constitutes the most difficult problem of manufacturing, as explained below. The chromatic dispersion mentioned in Section 2.2, paragraph (ii), is reduced by a correcting system. For all optical elements the tolerances needed for the quality of the surfaces, for the radii of curvature, and for the positioning, tilt and eccentricity, etc., have been assessed with computer simulation of CEDAR performances.

3.1.1 Chromatic corrector

The most flexible system is a composite lens with quartz and sodium chloride axicones, which does not deflect the central wavelength (see Fig. 9a). By locating it at various distances from the focal plane, one varies the compensation in relation to the gas pressure. This solution has been adopted for the DISC counter¹⁾ made for FNAL, but is complex and expensive.

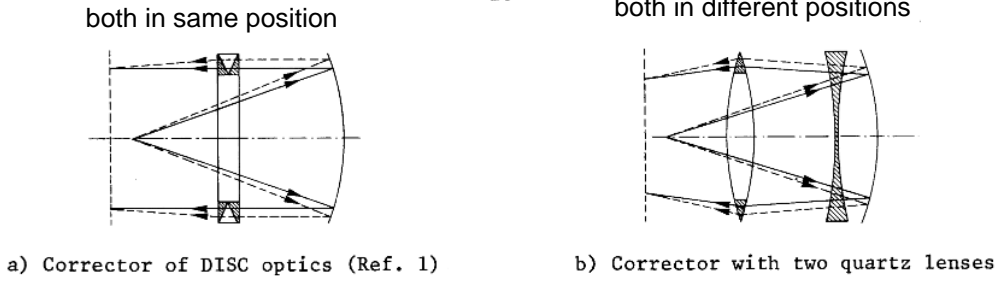
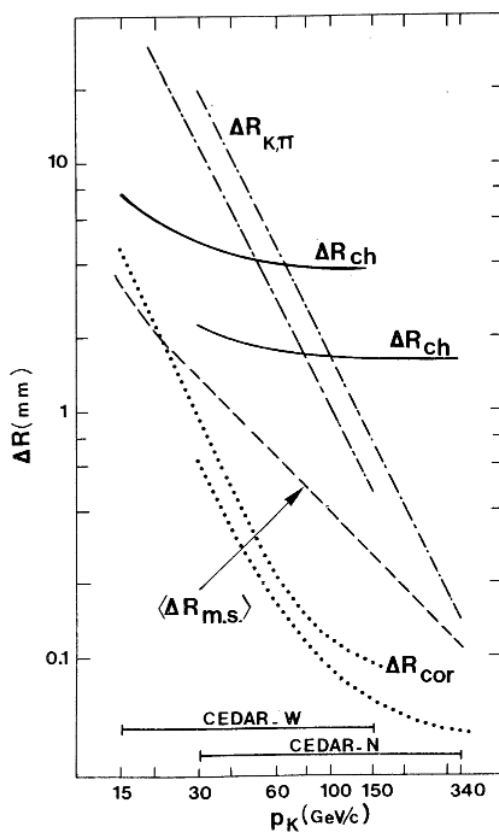


Fig. 9 Chromatic corrector optics

If one accepts the use of only one kind of gas in a given counter, the chromatic dispersion only depends through Eq. (6) upon γ of the wanted particle. Therefore a fixed corrector can be designed to best compensate for the chromaticity when the ultimate resolution must be achieved, i.e. for separation of kaons and pions of the highest momentum. With decreasing momentum (higher gas pressure) the chromatic dispersion gets larger and is only partially compensated by the fixed corrector, but the separation between the light rings increases faster than the spot size as can be seen from Fig. 10.

This solution has been adopted and, in order to cure both transversal and longitudinal chromatic aberrations, two quartz lenses are needed. The first lens can be associated with the mirror, which becomes a Mangin mirror (back surface reflecting) (see Fig. 9b). This mirror has a central hole of 100 mm diameter to let the beam through. These optical elements are shown in real proportions in Fig. 11.



When the best correction is achieved it still provides only a first-order cancellation [the curvature of the dispersion function $n(\lambda)$ is not the same for He and SiO_2 , nor for N_2 and SiO_2]. Thus a second-order dispersion remains, which grows rapidly towards the UV region. To strike a balance between maximum light output and best resolution we have set a cut-off at $\lambda = 240$ nm by means of glass filters glued onto the exit windows.

Fig. 10 CEDAR resolution. For both CEDAR-W and CEDAR-N the chromaticity ΔR_{ch} and its remanent value after correction ΔR_{cor} are compared with the separation between pions and kaons $\Delta R_{K,\pi}$ and the effect of the multiple scattering undergone by the beam $\langle \Delta R_{ms} \rangle$.

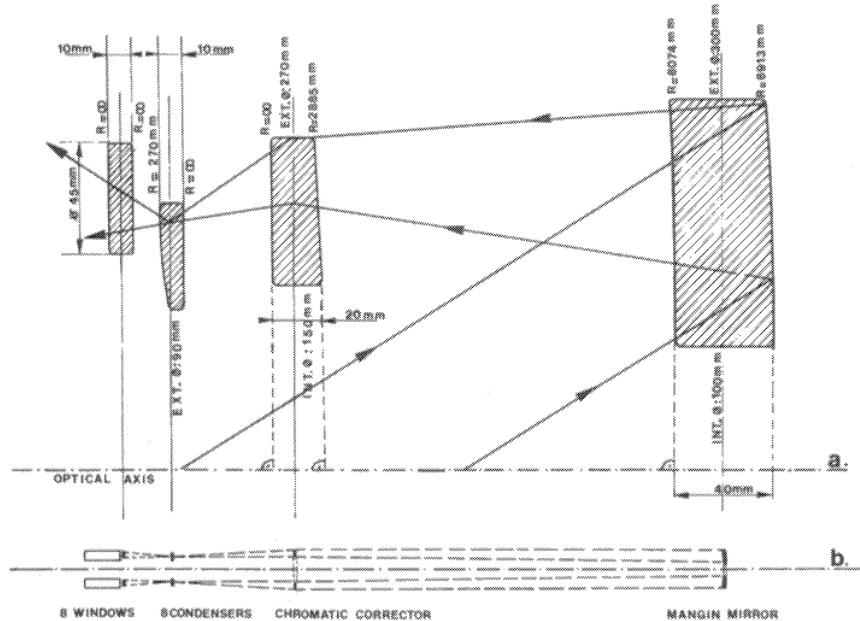


Fig. 11 a) CEDAR optical elements enlarged to better show their real shape and located in a distorted scale drawing of the optical trajectories. b) CEDAR optics on a real scale.

3.1.2 Mangin mirror

Strict tolerances have been put on the quality of the quartz blanks (300 mm diameter and 40 mm thickness) in which the mirrors are polished. A path length homogeneity of $\lambda/8$ was required. Only one supplier has offered to produce quartz pieces of such dimensions and quality, and the acceptance of these blanks has been subjected to the analysis of double path interferometry in order to determine the inhomogeneities in terms of spherical aberrations and astigmatism, see Ref. 3. The quality required was not quite met by all the blanks and spherical polishing would not have produced mirrors with the wanted performance. But some aspherical figuring could be done on the back surface of the mirrors to help to correct for the quartz imperfections. As a final test, double traversal analysis with the scatter fringe method was made to check the quality achieved (Fig. 12). Behind the diaphragm eight simple condenser lenses focus the light onto the photomultipliers. Table 2 shows the main parameters of these optical elements.

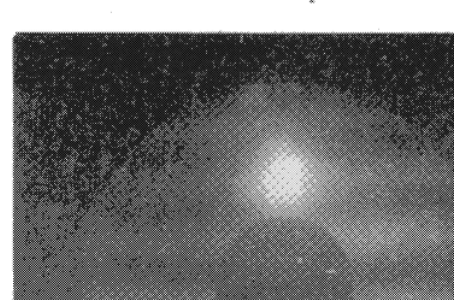


Fig. 12 Scatter fringe interferogram taken at the functional focus of the Mangin mirror



Table 2
Optical parameters list

	CEDAR-W	CEDAR-N
Mirror		
Glass	Suprasil I	Suprasil I
Outer diameter	300 mm	300 mm
Hole diameter	100 mm	100 mm
Radius of reflecting surface	8610 mm	8913 mm
Radius of refracting surface	6615 mm	8074 mm
Thickness	40 mm	40 mm
Corrector		
Glass	Suprasil I	Suprasil I
Outer diameter	320 mm	270 mm
Hole diameter	150 mm	150 mm
Thickness	20 mm	20 mm
Radius of entrance surface	1385 mm	2885 mm
Radius of exit surface	> 5000 m	> 5000 m
Condensers		
Glass	Spectrosil	Spectrosil
Thickness	10 mm	10 mm
Radius of entrance surface	300 mm	270 mm
Radius of exit surface	∞	∞
Radial eccentricity	30 mm	10 mm

3.1.3 Optical tests

For every CEDAR's optics the optimum longitudinal positions of the lenses have been computed with the measured radii of curvature. The system was then tested with a light source put at the height of the diaphragm, by collecting the light through a movable slit on the other side of the diaphragm (Fig. 13). In this process the light is reflected on a test mirror of quality $\lambda/15$ and simulates a Čerenkov emission. This double path through the whole optical system gives a high sensitivity to measure defects or mismatches that result in an increase of the spot size. Such measurements allowed us to establish the focal

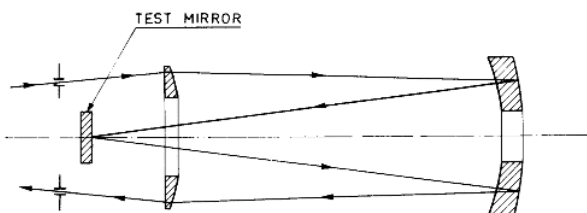


Fig. 13 Diagram of light path for optical test of the assembled system

length of the system to within 1 mm, and once this information was available another computer optimization was carried out to define the final position of the mirror and of the corrector.

3.1.4 Light output

It is interesting to note that, as shown in Fig. 14, the mirror diameter has not to be made larger than 300 mm for the benefit of off-axis particles, since there is no point in collecting more photons in the already favoured sectors 1 to 4, as shown by the shaded area in the example of Fig. 15.

The range of the photon spectrum which can be accommodated is described in Section 3.1.1 above and is limited by the needs for high resolution. The back surface of the mirror is coated with Alflex UV covered by a protecting layer, and a high reflectivity of up to 90% has been obtained. All refracting surfaces are treated with MgF_2 (a 75 nm thick layer) for a minimum reflection at 300 nm. A very good transmission efficiency for the total quartz thickness of 120 mm is achieved with Suprasil I and Spectrosil A. All effects contributing to the effective spectrum are illustrated in Fig. 16.

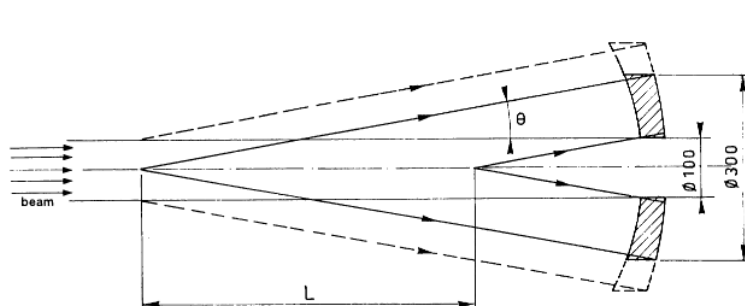


Fig. 14 Effective radiator length for a hollow mirror

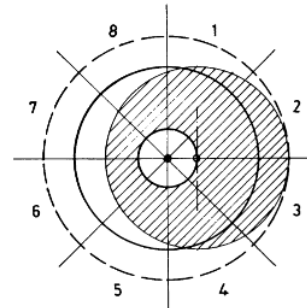


Fig. 15 Photon distribution on the mirror from a particle belonging to the edge of the beam

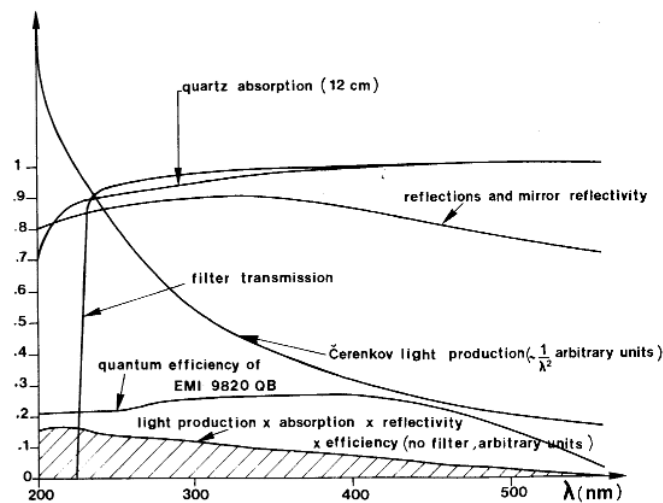


Fig. 16 Light production, transmission, and detection versus photon wavelength

3.2 Mechanical engineering

The pressure vessel (15 bar) is made of a steel pipe with 534 mm inner diameter and 558 mm outer diameter, welded on square flanges, to which a nose with eight quartz windows and photomultipliers is bolted on the upstream end while a spherical head closes the downstream end (see Appendix C).

3.2.1 Temperature uniformity

In order to achieve a temperature uniformity of ± 0.1 K, as required in the most extreme conditions (see Section 3.3.1), the whole counter is packed with 100 mm of polyurethane foam to provide the best thermal insulation. The supporting feet, gas pipes, and electric cables are designed to minimize thermal conduction to the outside world. In order to improve the longitudinal conductivity, thick aluminium shells have been clamped to the outside of the big vessel and copper shells are fastened onto the nose. With these improvements the time constant for heat diffusion along the counter is reduced to less than a day and the daily variations of the external temperature are attenuated by a factor of 20. The vessel temperature is monitored by three platinum wire thermometers located at both ends and at the diaphragm main flange. Temperature gradients of $\Delta T \geq 0.3$ K have been monitored only exceptionally after a big seasonal temperature change in the halls.

3.2.2 Windows

The beam traverses the counter through circular windows made of aluminium alloy (norm AFNOR = AZ5GU) with a diameter of 100 mm and a thickness of 0.4 mm. These membranes are hydroformed in the hard state to reach a radius corresponding to the equilibrium sphere for the elastic limit of their material. Samples have undergone a life test, being cycled from 1 to 45 bar 2000 times with a rise-time of 0.1 s. The tightness is obtained with all metallic contacts of the membranes on bolted flanges machined with toroidal surfaces.

The eight optical windows are made of quartz cylinders of 45 mm diameter and 10 mm thickness. Their ring frame is made of stainless steel and the binding is obtained by heating the rings at 150 °C. When the ensemble is cooled down, the layer of silver deposited on the circumference of the quartz disk is compressed and produces a perfect sealing. A destructive test was made whereby 300 bar were reached.

3.2.3 Optical tower

The supporting structure holding the mirror, the chromatic corrector, and the diaphragm is an isostatic triangular assembly of tubes bolted on spherical cups. The tower is straight to within ± 0.2 mm over 4.5 m and has a static sag of 0.1 mm. It is supported by a sphere under the diaphragm and is fixed without constraint to the pressure vessel so that pressure or temperature variations do not affect the optical axis. The ring diaphragm is located at the upstream end of the tower. The mirror frame, fixed at the downstream end, provides for mirror alignment in both radial and longitudinal directions. The chromatic corrector rests on the first intermediate ring of the tower and can also be aligned in three directions.

3.2.4 Ring diaphragm

The diaphragm is composed of a disk with 8 elongated apertures and 8 outer and 8 inner segments moved by right-left screw drives. The segments are bolted on high-precision guided

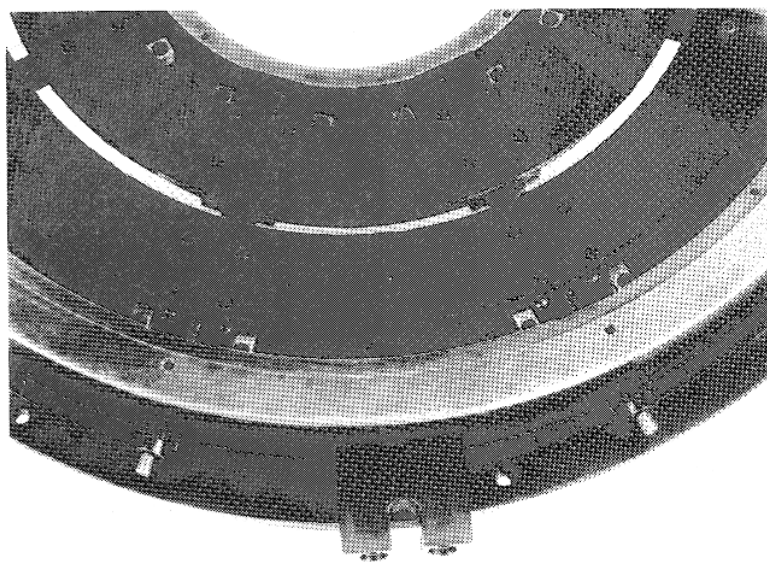


Fig. 17 Photograph of the light diaphragm where two of the eight sectors can be seen

chariots. The 8 screw drives are provided with gears and are turned simultaneously by a gear mounted on ball bearings in a V-groove on the periphery of the disc (see Fig. 17). The opening can be varied between 0.03 mm and 20 mm, in steps of 0.01 mm, with a motor located externally to the vessel. A final check of the circularity of the aperture performed on an optical turntable shows radial deviations of less than 0.02 mm.

3.2.5 Alignment table

The fine alignment of the optical axis with the beam axis is made by rotating the whole counter. To provide for this motion the pressure vessel is supported on three points: one sphere located under the diaphragm and two spheres whose bases are resting on a V-shaped surface under the mirror. The alignment mechanism made of cast aluminium has two chariots moved by right-left screw drive, opening the V-surface. The motion of these chariots in opposite directions produces a vertical displacement, whereas a motion in the same direction (horizontal displacement) is provided by another screw drive. These fine displacements in the horizontal and vertical directions with a step resolution of 0.01 mm provide an angular positioning within 2 μ rad. For all these mechanical parts relevant parameters are listed in Table 3.

3.3 Gas controls

In order to achieve the best mass resolution, the index of refraction must be uniform

Table 3
Mechanical parameters list

Overall length	6200 mm
" width	920 mm
" height	1890 mm
" weight	2.4 t
Beam windows:	
material	Aluminium alloy
diameter	100 mm
thickness	0.4 mm
Optical tower:	
length	4500 mm
sag due to gravity	0.1 mm
thermal expansion	0.05 mm/K
Diaphragm:	
azimuthal opening	$8 \times 42.6^\circ$
radial opening (LD)	0 to 20 mm
opening accuracy	0.01 mm
Alignment table:	
x, y range	-4.3 to +4.3 mm
$\Delta x, \Delta y$ accuracy	0.01 mm
angular resolution	2.3 μ rad

in the whole radiator and stable during the period of data taking. The first condition requires an excellent uniformity of temperature, which is obtained by the means explained in Section 3.2.1, but it does not imply that this average temperature has to be kept constant in time. The second condition requires a perfect tightness of the vessel and/or an easy way of restoring the wanted index of refraction, by tuning the pressure to follow the volume variations of the vessel due to temperature changes.

3.3.1 Measurement of the index of refraction

The variations of the index of refraction must be kept, say, ten times smaller than the ultimate resolution $\Delta\beta/\beta = 10^{-6}$, in order to match the quality of the optical system. One therefore aims at keeping the index of refraction within $\Delta n/n \leq 10^{-7}$. Although it is possible to build a refractometer with this resolution (see Ref. 4), it was not felt desirable to have refractometers of that quality and complexity attached to each of the twelve CEDARS operating in the SPS areas. The chosen alternative was to monitor the density of the gas through pressure and temperature. Indeed the index of refraction can be deduced from the density since a unique gas is used with each type of counter.

The index of refraction of a gas can be expressed in terms of electron oscillators as

$$n - 1 = \frac{Nq_e^2}{2\epsilon_0 m} \sum_k \frac{f_k}{\omega_k^2 - \omega^2 + i\gamma_k \omega}, \quad (18)$$

where N is the number of atoms per unit volume⁵⁾. Clearly $n - 1$ is proportional to the gas density and, using the perfect gas equation, this then reads:

$$n - 1 = (n_0 - 1) \left(\frac{T_0}{P_0} \right) \frac{P}{T}, \quad (19)$$

where P and T are the actual pressure and temperature, and n_0 is measured at $P_0 = 1$ bar and $T_0 = 293$ K.

The error propagation obtained by differentiation of Eq. (19) reads:

$$\frac{\Delta n}{n} = \frac{(n - 1)}{n} \left[\frac{\Delta P}{P} - \frac{\Delta T}{T} \right]. \quad (20)$$

Since $(n - 1)/n \approx 1/3000$ (see Table 4), the accuracy needed to monitor P and T is 3000 times smaller than the accuracy required to measure n directly. Tolerances on n , P , and T , corresponding to the wanted resolutions, are listed in Table 4.

Table 4
Tolerances and accuracies for gaseous state

CEDAR type	θ (mrad)	$\frac{n}{n - 1}$	Ultimate separation ($\Delta\beta/\beta$) _{sep}	Corresponding accuracies			
				$\Delta\beta/\beta$	$\Delta n/n$	$\Delta P/P$	ΔT (K)
W	30.9	2095	5×10^{-6}	5×10^{-7}	5×10^{-7}	10^{-3}	0.3
N	25.8	3005	10^{-6}	10^{-7}	10^{-7}	3×10^{-4}	0.1

In practice, the measurement of the temperature is straightforward, but the precautions explained in Section 3.2 are needed to obtain a uniformity of temperature along the vessel. To measure the pressure a precise instrument is required, which is calibrated in the laboratory with a reference refractometer.

The slight contamination of the gases (N_2 or He), due to leaks of the windows or coming from outgassing of the counter vessel, can be dealt with.

3.3.2 Gas pressure monitoring and absolute calibration

The heart of the pressure control is a very accurate pressure transducer⁶⁾, which provides, with a stability of 10^{-4} , an electrical wave form whose frequency is related to the pressure of the gas (so that a measurement of pressure is reduced to a measurement of a frequency). The principle of operation of these transducers^{*)} is briefly illustrated below. The sensing elements consist of two concentric cylinders, a vibrating inner one and a protective outer one. A spool body internal to the inner cylinder holds small electromagnets which drive the vibrating cylinder and pick-ups to detect its motion and frequency. The space between the two cylinders is evacuated to give an absolute pressure reference. The volume between the inner cylinder and the spool body is pressurized with the gas to be measured and this causes the cylinder's natural frequency to increase. The frequency is detected by the pick-up, which provides a square wave voltage whose frequency is proportional to the pressure of the gas. The whole transducer is thermostatted at 40 ± 0.5 °C in order to avoid the frequency swing due to external temperature.

Each pressure transducer is calibrated⁷⁾ by means of a Rayleigh-type refractometer in the laboratory. For each pressure point the index of refraction is established by counting the fringes for the optical path difference between an evacuated cell and a cell filled with the gas for which pressure and temperature are recorded simultaneously. A typical number of fringes is ten thousand and the high accuracy is obtained by sharp interpolation by means of an array of sixteen light diodes.

The frequency response of the Hamilton transducer is not linear in pressure and a fit is made for each transducer of a polynomial with six parameters⁷⁾.

3.3.3 Gas handling

Each CEDAR is connected to the gas supply network of nitrogen or helium, where a pressure of 20 bar is available. On the feeding line the pressure is automatically kept at a value of $P+5/P$ (bar), with a spring-biased pressure regulator. Similarly a pressure of 1.5 bar is maintained on the outlet branch so that equal quantities of gas can be let in or out by activating on/off valves for a controlled time. In this way the gas pressure can easily be computer-controlled. A gas expansion of less than $5/P$ (bar) at the inlet is important to keep the temperature uniformity needed for the best resolution [see Section 5.3, paragraph (vi)].

^{*)} This instrument is now distributed by The Solartron Electronic Group Ltd., Farnborough, Hampshire, England.

4. LAYOUT, ELECTRONICS, AND COMPUTER CONTROLS

4.1 Layout

The angular acceptance of CEDARS is very small when the light diaphragm is closed to ensure the best separation. Therefore the SPS secondary beams have been designed including a section with the best parallelism (large beam dimensions and small divergence in both horizontal and vertical planes) for the installation of CEDARS, in order to optimize the counting efficiency.

One or two CEDARS can be installed in such sections and the basic layout, shown in Fig. 18, consists of:

- 2 scintillation counters XTRI 1, XTRI 2 (\varnothing 100 mm, 5 mm thick NE 110),
- 1 anticounter XANT (with a circular hole of \varnothing 100 mm) in front of each CEDAR,
- 1 two-plane (horizontal and vertical) analog wire chamber XWCA⁸ ,
- 2 pairs of filament scintillation counters⁹) XFSs.

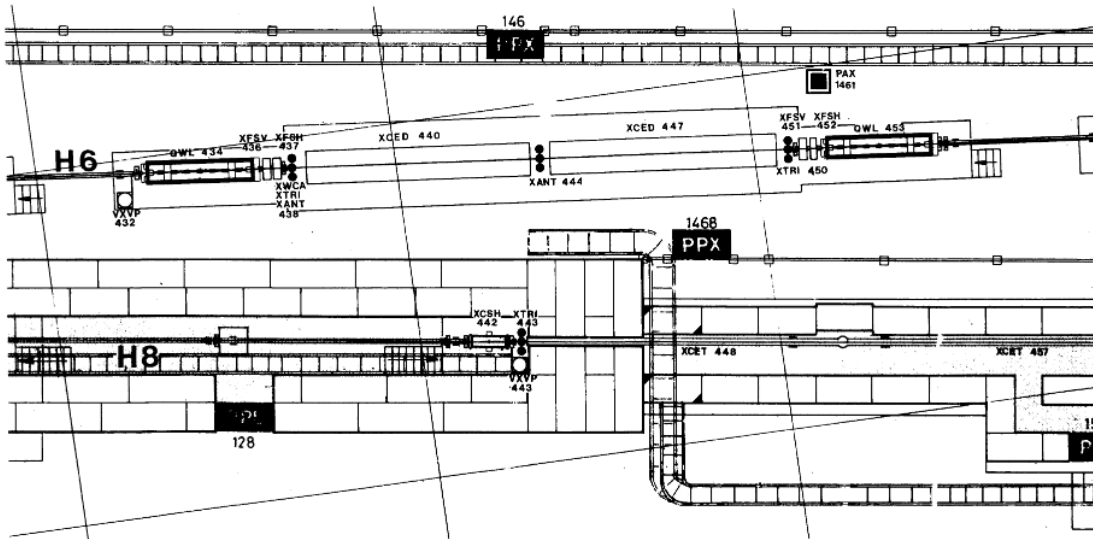


Fig. 18 Typical layout of two CEDARS and associated equipment in a beam line (H6)

The two XTRIs are used in coincidence to define the useful beam region. The counters XANT are used to veto halo particles which travel outside the useful beam (their use is recommended when working at beam intensities of 5×10^6 or more). The wire chambers XWCA are used to measure the beam position and size at the CEDAR during the tuning of the beam. The two pairs of XFSs (horizontal and vertical filament beam scanners) are finally used to adjust the beam direction and parallelism, by operating them in coincidence⁹). The trigger counters, the wire chamber, and the scintillator filaments of the XFSs must be taken out of the beam during data taking (remote control).

4.2 Electronics for signal treatment

The block diagram of the electronics associated with each CEDAR is shown in Fig. 19. The signals from the 8 photomultipliers are first shaped by fast discriminators operated at

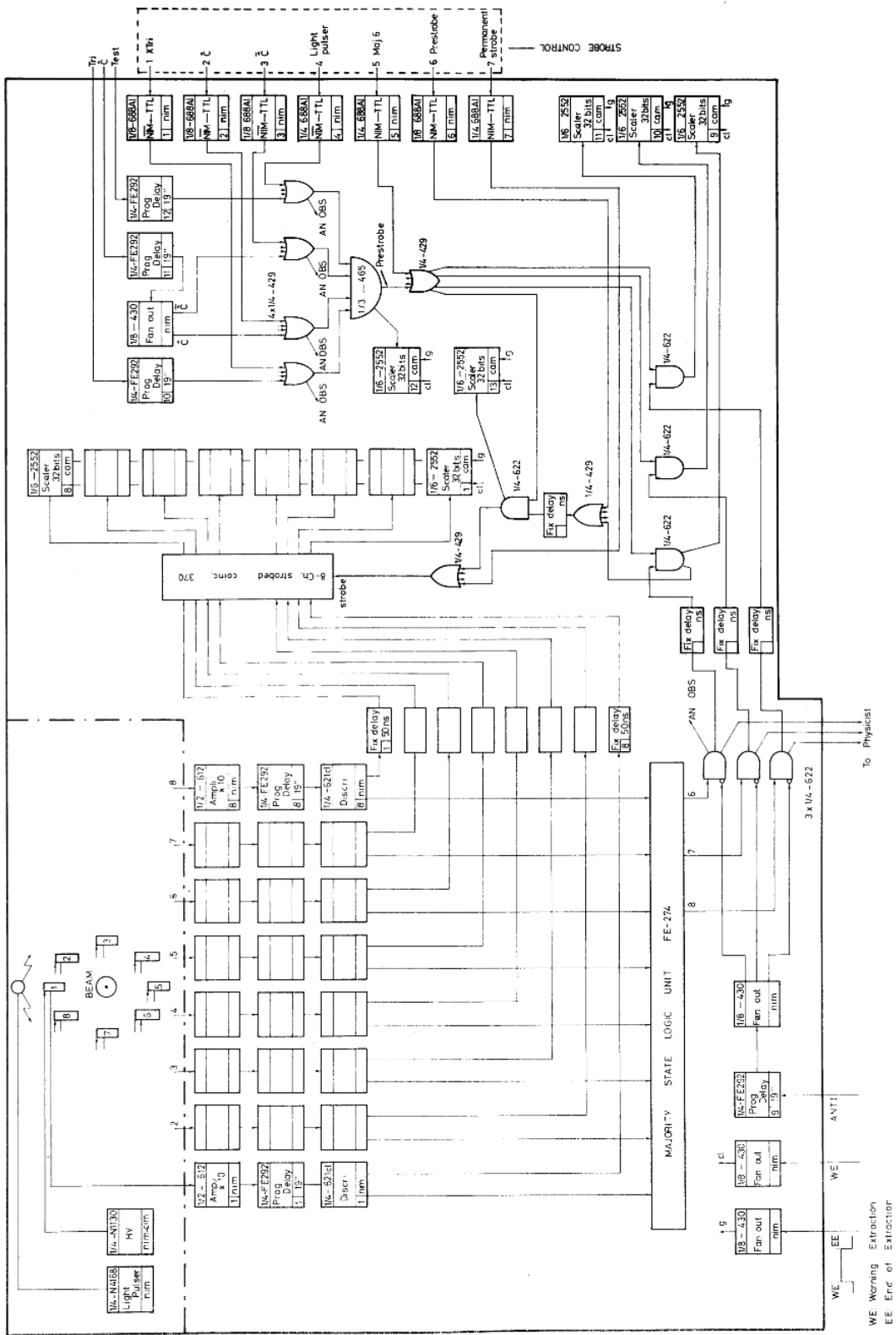


Fig. 19 Block diagram of CEDAR electronics

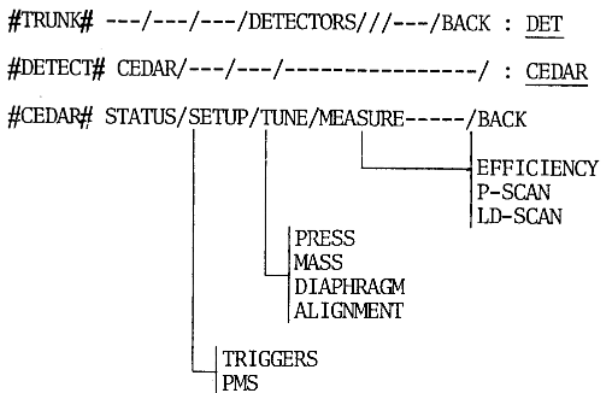
low threshold to detect one single photoelectron, and then split into two. One signal goes to a majority state logic unit where three levels of coincidence (sixfold, sevenfold, and eightfold) are provided and sent to the experimenters, usually in anticoincidence with the XANT signal. The other signal is used for the diagnostics of the instrument. The signals of each photomultiplier are sent to a strobed coincidence unit and recorded on 8 scalers. When the two XTRI trigger counters are introduced into the beam, their coincidence signal is used as a strobe input; the counts read in the 8 scalers give information on the efficiency of each photomultiplier and on the size and position of the light-ring image at the diaphragm plane.

To complete the CEDAR diagnostics, the counts of the sixfold, sevenfold, and eightfold coincidences are also recorded; they are used to evaluate the average number of photoelectrons (NPE) seen by the photomultipliers (NPE is deduced from the ratio of the rates counted at the three levels of coincidence, which can be done even when the trigger counters are not in the beam, see Appendix A), and to measure the mass spectra and the rejection of unwanted particles while scanning the CEDAR gas pressure.

4.3 Computer controls

All CEDARS installed in the SPS secondary beams can be operated simultaneously from the EA computer terminals installed in the experimenters' counting rooms via a set of control and diagnostic programs.

For that purpose a series of interacting programs have been written to help in tuning and operating each CEDAR. They can be run under the program (TREE) associated with the beam line in use. The sequence in which these different programs can be reached and the several options are listed below:



A description of the subroutines is given in the following. The algorithm used is as shown in Appendices A and B.

STATUS is an acquisition program which reads and displays the current values of the parameters of the detector useful for its control and operation. A typical example of its write-out is shown below.

```
* DETECT # CEDAR/THRESH/MVPC/FISC/TRIG/SPECTR/ATRIG/HODOSC/SPILL/EXPT/.CEDAR
CEDAR IN THIS BEAM: 2
NUMBER :1

* CEDAR # STATUS/SETUP/TUNE/MEASURE////BACK/.ST

STATUS OF # CEDAR - 1 # IN BEAM HG AT -150 GEV/C 1982-04-28-21:08
*****
* GAS TEMPS # HEAD = 22.50 [DEG] \
MID = 22.35 [DEG] > MAX. TEMP. DIFF.= .30 [DEG]
TAIL = 22.20 [DEG] /
TRANSDUCER IS OK = 39.47 [DEG] ROOM = 23.49 [DEG]

* PRESS AND MASS # PRESS= 10.3278 [BAR] MASS= .469 +/- .003 [GEV]

* MASS-PRESS # ELECTRONS=10.178 [BAR] MUONS =10.185 [BAR]
PIONS=10.191 [BAR] KAONS =10.343 [BAR] PROTONS=10.776 [BAR]
* MOTORS POS. #
DIAPHRAGM= 1.00 [MM] * HOR. X = .88 [MM] * VERT. Y = .30 [MM]

* TRIGGERS POS. # TRIGGERS ARE IN HV IS ON

* PMS # EFF'S (6)=9.60E-1 EFF'S (7)=8.10E-1 EFF'S (8)=4.26E-1
TRIGGERS =2.38E6 NPE/PM =2.29
*****
HARDCOPY (Y/RET):
```

#GAS TEMPS# gives the gas temperatures in three sections of the vessel; their average value is used with the gas pressure to evaluate the actual index of refraction of the radiator. The body temperature of the pressure transducer (Section 3.3) is also given. A warning message is issued in the case of an abnormal value, since in that condition the transducer information is wrong.

#PRESS AND MASS# gives the actual average gas pressure and the calculated value of the mass on which the detector is tuned at that time.

#MASS-PRESS# gives the computed gas pressures which should be used, in accordance with the actual gas temperature, to tune the CEDAR on the masses of e, μ , π , K, and p for the current beam momentum.

#MOTOR POS# gives the light diaphragm opening and the position (horizontal and vertical) of the alignment table.

#TRIGGER POS# checks the position of the triggers in the beam and if their high voltage is on or off, without modifying any of these parameters.

#PMS# evaluates the sixfold, sevenfold, and eightfold efficiencies from the measured average NPE per photomultiplier -- Appendix A -- and from the beam intensity (TRIGGERS).

SETUP reads and displays the parameters (delay and photomultiplier high voltage) of the triggers associated with the CEDAR (TRIGGERS) and those of the CEDAR itself (PMS). Both subroutines allow the high voltage of the photomultipliers to be switched off or to be restored to the reference values. The TRIGGERS branch also permits the triggers to be taken out of the beam when the CEDAR is ready for data taking.

```
*SETUP# :TRIGGERS/PMS/ :TR
TRIGGERS OF CEDAR - 1 # IN BEAM H6 AT -150 GEV/C      1982-04-28-21:10
*****
```

*POS. TRIGGERS # TRIGGERS ARE IN

TRIGGER	DELAY[NS]	HV[KV]	SCALER
UPSTR	-1	1.82	2.17E6
DOWNSTR	29	1.91	2.15E6

TRIGGERS # WANT THEM IN BEAM (Y/N):Y

TRIGGERS PMS # RESTORE/ZEROHV (R/Z):

```
*SETUP# :TRIGGERS/PMS/ :PMS
```

```
PMS CEDAR - 1 # IN BEAM H6 AT -150 GEV      1982-04-28-21:11
*****
```

* TRIGGERS POS. # TRIGGERS ARE IN

PM NUMBER	DELAY[NS]	HV[KV]	SCALER
1	0	1.71	5.79E5
2	11	2.51	5.66E5
3	10	2.10	5.20E5
4	6.5	1.74	3.31E5
5	15	2.01	5.51E5
6	8	2.40	8.73E5
7	12	2.20	1.08E6
8	14	2.21	9.02E5
6-FOLD	0	*****	1.14E5
7-FOLD	7	*****	9.49E4
8-FOLD	0	*****	5.84E4
TRIGGERS-COINC	0	*****	2.46E6

CEDAR PMS # RESTORE/ZEROHV (R/Z):

TUNE is an active program by which one can tune the CEDAR through the routines:

PRESS/MASS/DIAPHRAGM/ALIGNMENT

- PRESS measures the current gas pressure; then a different value in the permitted range can be requested. The new value is measured at the end of the operation. The write-out is self-explanatory.
- MASS evaluates the mass which could be detected with the current value of the index of refraction (Appendix B) together with its uncertainty, then a new value can be asked for. The print-out is similar to PRESS.
- DIAPHRAGM is the same as the previous routines.
- ALIGNMENT allows alignment of the optical axis of the detector on the average beam direction. This is achieved by using the XY alignment table (Section 3.2.5), which supports the downstream end of the counter. The range of displacement of the XY table is ± 4.3 mm with an accuracy of 0.02 mm in both directions, which allows the CEDAR optical axis to be moved inside a cone of 1 mrad semi-aperture with an accuracy of 4 μ rad to get the best matching with the beam direction. A typical print-out of this routine is shown below.

ALIGNMENT CEDAR - 1 - IN BEAM H6 AT -150 GEV/C . 1982-04-28-21:23

TRIGGERS POS. # TRIGGERS ARE IN

PRESS=10.3278 [BAR] MASS = .469 +/- .003 [GEV]

TRIGGERS = 2.09E6 NPE/PM= 2.29

DIAPHRAGM = 1.00 [MM]
HOR X = .80 [MM]
VERT Y = .30 [MM]

2 PM/TRI			2 PM /MEAN		
*****			*****		
8	35	24	1		(U)
7	42	24	2	R/L = .61	109
6	34	22	3	U/D = 1.66	(L) 139 85 (R)
5	21	14	4		65
					(D)

CHANGE ALIGNMENT (YES/RET):

As a first step the two triggers are positioned in the beam and the actual status of the detector is given (gas pressure and motor positions). The counting rates of the eight photomultipliers, normalized to the beam intensity (TRIGGERS), are then displayed according to their position in the counter (beam entering the screen).

The ratios

$$\frac{R}{L} = \frac{2 + 3}{6 + 7}, \quad \frac{U}{D} = \frac{1 + 8}{4 + 5}$$

are shown in the central part, while in the right-hand part of the screen the eight counting rates are grouped (R = 2 + 3, etc.) and normalized to the average of them all.

ALIGNMENT CEDAR - 1 - IN BEAM H2 AT 250 GEV/C 1981-09-25-11:59

8 38 36 1	CEDAR #1 H2 250 GEV * TRIG= 3.94E5	* 2 PM/MEAN *
7 76 70 2	U/D = 2.93 R/L = 1.01 NPE/PM= .76	85
6 46 54 3	X = -.84*Y = 2.79*DIA = .29 [MM]	141 143
5 9 16 4	M= .932 [GEV] - 1- P= 10.4131 [BAR]	29
8 69 66 1	CEDAR #1 H2 250 GEV * TRIG= 3.79E5	* 2 PM/MEAN *
7 77 73 2	U/D = 1.79 R/L = 1.03 NPE/PM= 1.31	113
6 54 62 3	X = -.84*Y = 2.90*DIA = .29 [MM]	109 113
5 30 45 4	M= .932 [GEV] - 2- P= 10.4131 [BAR]	63
8 77 73 1	CEDAR #1 H2 250 GEV * TRIG= 1.78E5	* 2 PM/MEAN *
7 75 73 2	U/D = 1.34 R/L = 1.12 NPE/PM= 1.66	112
6 52 70 3	X = -.84*Y = 2.95*DIA = .29 [MM]	95 107
5 44 67 4	M= .932 [GEV] - 3- P= 10.4131 [BAR]	84
8 78 76 1	CEDAR #1 H2 250 GEV * TRIG= 3.74E4	* 2 PM/MEAN *
7 72 73 2	U/D = 1.12 R/L = 1.10 NPE/PM= 1.89	109
6 56 69 3	X = -.84*Y = 2.99*DIA = .29 [MM]	91 101
5 61 76 4	M= .932 [GEV] - 4- P= 10.4131 [BAR]	97
8 79 77 1	CEDAR #1 H2 250 GEV * TRIG= 3.07E5	* 2 PM/MEAN *
7 75 74 2	U/D = 1.12 R/L = 1.08 NPE/PM= 1.93	108
6 59 70 3	X = -.84*Y = 3.01*DIA = .29 [MM]	93 101
5 62 76 4	M= .932 [GEV] - 5- P= 10.4131 [BAR]	96

```

8 79 78 1 CEDAR #1 H2 250 GEV * TRIG= 3.01E5 * 2 PM/MEAN *
7 73 75 2 U/D = .99 R/L = 1.06 NPE/PM= 2.12 104
6 65 72 3 X = -.84XY = 3.05*DIA = .29 CHM1 91 98
5 75 82 4 M= .932 [GEV] - 6- P= 10.4131 [BAR] 104
***** * 2 PM/MEAN *
8 79 77 1 CEDAR #1 H2 250 GEV * TRIG= 1.65E5 * 2 PM/MEAN *
7 75 72 2 U/D = .98 R/L = .96 NPE/PM= 2.15 103
6 70 69 3 X = -.90XY = 3.05*DIA = .29 CHM1 96 93
5 77 81 4 M= .932 [GEV] - 7- P= 10.4131 [BAR] 105
***** * 2 PM/MEAN *
8 79 78 1 CEDAR #1 H2 250 GEV * TRIG= 2.46E5 * 2 PM/MEAN *
7 73 73 2 U/D = .98 R/L = 1.02 NPE/PM= 2.14 104
6 67 71 3 X = -.87XY = 3.05*DIA = .29 CHM1 93 96
5 76 82 4 M= .932 [GEV] - 8- P= 10.4131 [BAR] 105
***** * 2 PM/MEAN *

```

MEASURE allows the efficiency of the CEDAR to be measured and a pressure scan (SCAN) to be performed in order to define the working point more accurately.

- EFFICIENCY displays the measured sixfold, sevenfold, and eightfold counting rates normalized to the beam's total intensity (TRIGGER); the related efficiencies evaluated as described in Appendix A are then shown.
- P-SCAN is a subroutine which performs a gas-pressure scan between two given limits and with a given number of steps. After every step the sixfold, sevenfold and eightfold majorities are acquired, but the display is given only when the required statistics (TRIG) has been reached.

The NPE per photomultiplier is evaluated from the three levels of coincidence (see Appendix A) and is quoted together with the ratio R between the two results for NPE, which should be ~ 1 in the case of good statistics.

A typical print-out is shown in the following, where the gas pressure scan has been performed decreasing the CEDAR pressure in order to perturb the thermal equilibrium of the gas as little as possible. The scan limits have been chosen in order to locate the K^+ and π^+ peaks.

The slight differences between the pressure values corresponding to the peaks and those theoretically predicted are due to changes in the gas purity and can be duly corrected.

P(E)=10.244 P(MU)=10.248 P(PI)=10.251 P(KA)=10.338 P(P)=10.583 BAR

CEDAR# 1 IN BEAM H2: SCAN FROM 10.401 TO 10.15 BARS; STEP= -4.16 MBAR
L D= .405 MM; MOMENTUM:-200 GEV/C 1979-08-12-14:43:53

PRESS [BAR]	TRIG	NPE/PM	R	MAJORITIES			CYCLE	MEAS
				6-FOLD	7-FOLD	8-FOLD		
10.4013	1.88E5	*	*	1.54E-5	5.35E-6	5.35E-6	2	1
10.3975	1.82E5	*	*	1.05E-8	1.05E-8	1.05E-8	2	2
10.3943	2.00E5	*	*	9.90E-9	9.90E-9	9.90E-9	2	3
10.3919	1.74E5	*	*	5.17E-5	1.13E-8	1.13E-8	2	4
10.3884	1.83E5	.04	.28	9.29E-5	5.48E-6	1.02E-8	2	5
10.387	2.27E5	.02	.15	2.05E-4	1.31E-5	8.82E-9	2	6
10.3839	1.71E5	.70	2.15	6.19E-4	3.51E-5	5.80E-6	2	7
10.3808	2.16E5	.45	1.21	1.82E-3	1.83E-4	1.34E-5	2	8
10.3784	2.27E5	.57	1.01	3.95E-3	7.64E-4	6.66E-5	2	9
10.376	1.92E5	.88	1.07	7.33E-3	2.07E-3	3.26E-4	2	10
10.3735	1.78E5	1.13	1.08	1.03E-2	4.05E-3	8.77E-4	2	11
10.3704	1.65E5	1.29	1.06	1.42E-2	6.57E-3	1.61E-3	2	12
10.3683	1.80E5	1.53	1.09	1.76E-2	8.98E-3	2.99E-3	2	13
10.3663	1.97E5	1.73	1.08	2.14E-2	1.26E-2	4.84E-3	2	14

10.3631	1.89E5	1.92	1.08	2.39E-2	1.55E-2	6.61E-3	2	15
10.3607	1.91E5	1.99	1.06	2.42E-2	1.64E-2	7.76E-3	2	16
10.3583	2.18E5	2.20	1.06	2.69E-2	1.98E-2	1.09E-2	2	17
10.3555	2.12E5	2.27	1.05	2.65E-2	2.01E-2	1.15E-2	2	18
10.3528	1.71E5	2.37	1.03	2.83E-2	2.34E-2	1.38E-2	2	19
10.3503	1.94E5	2.49	1.03	2.85E-2	2.45E-2	1.48E-2	2	20
10.3472	2.12E5	2.62	1.02	2.90E-2	2.54E-2	1.52E-2	2	21
10.3452	1.62E5	2.70	1.03	2.89E-2	2.45E-2	1.62E-2	2	22
10.3424	1.98E5	2.75	1.02	2.94E-2	2.68E-2	1.78E-2	2	23
10.34	1.98E5	2.79	1.01	2.97E-2	2.74E-2	1.77E-2	2	24
10.3376	1.71E5	2.80	1.02	2.90E-2	2.65E-2	1.75E-2	2	25
10.3348	1.98E5	2.82	1.02	2.93E-2	2.68E-2	1.74E-2	2	26
10.3324	1.92E5	2.75	1.01	3.00E-2	2.79E-2	1.75E-2	2	27
10.33	2.20E5	2.66	1.01	2.99E-2	2.68E-2	1.66E-2	2	28
10.3275	2.07E5	2.63	1.03	2.99E-2	2.54E-2	1.62E-2	2	29
10.3248	2.10E5	2.52	1.03	2.84E-2	2.44E-2	1.41E-2	2	30
10.322	1.97E5	2.42	1.03	2.82E-2	2.34E-2	1.35E-2	2	31
10.3199	1.60E5	2.32	1.03	2.77E-2	2.29E-2	1.20E-2	3	32
10.3175	1.79E5	2.20	1.05	2.66E-2	2.03E-2	1.09E-2	2	33
10.3144	1.85E5	2.03	1.04	2.53E-2	1.80E-2	8.58E-3	2	34
10.3117	1.73E5	1.86	1.07	2.43E-2	1.51E-2	6.42E-3	2	35
10.3093	1.56E5	1.75	1.06	2.38E-2	1.40E-2	5.44E-3	2	36
10.3068	1.96E5	1.51	1.06	1.93E-2	1.05E-2	3.39E-3	2	37
10.3041	1.69E5	1.26	1.05	1.74E-2	7.59E-3	1.81E-3	2	38
10.3017	2.02E5	1.05	1.08	1.52E-2	5.13E-3	1.02E-3	2	39
10.2993	1.76E5	.75	1.18	1.54E-2	2.91E-3	4.07E-4	2	40
10.2965	2.09E5	.42	1.15	2.34E-2	2.58E-3	1.61E-4	2	41
10.2941	1.49E5	.43	1.10	5.04E-2	5.94E-3	4.02E-4	2	42
10.2917	2.11E5	.64	1.10	1.17E-1	2.04E-2	2.28E-3	2	43
10.29	1.80E5	.84	1.07	2.07E-1	5.29E-2	7.71E-3	2	44
10.2863	1.94E5	1.12	1.11	3.04E-1	1.03E-1	2.37E-2	2	45
10.2841	2.02E5	1.31	1.09	4.15E-1	1.71E-1	4.63E-2	2	46
10.281	1.61E5	1.52	1.09	5.01E-1	2.57E-1	8.23E-2	2	47
10.2793	1.63E5	1.71	1.08	5.82E-1	3.31E-1	1.20E-1	2	48
10.2762	1.84E5	1.86	1.08	6.56E-1	4.17E-1	1.71E-1	2	49
10.2741	1.89E5	2.02	1.07	7.01E-1	4.86E-1	2.20E-1	2	50
10.271	1.81E5	2.16	1.06	7.55E-1	5.57E-1	2.81E-1	2	51
10.269	2.14E5	2.29	1.05	7.83E-1	6.07E-1	3.31E-1	2	52
10.2655	2.02E5	2.40	1.04	8.02E-1	6.55E-1	3.72E-1	2	53
10.2638	1.81E5	2.50	1.03	8.12E-1	6.81E-1	4.09E-1	2	54
10.2611	1.82E5	2.58	1.03	8.20E-1	7.14E-1	4.38E-1	2	55
10.2587	1.91E5	2.65	1.02	8.39E-1	7.35E-1	4.63E-1	2	56
10.2559	1.73E5	2.71	1.01	8.35E-1	7.49E-1	4.80E-1	2	57
10.2528	1.82E5	2.76	1.01	8.33E-1	7.57E-1	4.92E-1	2	58
10.2511	2.06E5	2.78	1.02	8.30E-1	7.56E-1	5.07E-1	2	59
10.2484	1.84E5	2.85	1.01	8.49E-1	7.72E-1	5.20E-1	2	60
10.2508	1.98E5	2.77	1.01	8.48E-1	7.68E-1	5.00E-1	2	1
10.246	1.65E5	2.71	1.02	8.39E-1	7.41E-1	4.81E-1	2	2
10.2412	2.03E5	2.63	1.02	8.34E-1	7.35E-1	4.50E-1	2	3
10.2371	1.81E5	2.52	1.03	8.23E-1	6.96E-1	4.13E-1	2	4
10.234	1.98E5	2.36	1.04	7.90E-1	6.32E-1	3.56E-1	2	5
10.2292	1.73E5	2.17	1.05	7.52E-1	5.60E-1	2.82E-1	2	6
10.2258	2.26E5	1.97	1.06	7.04E-1	4.83E-1	2.12E-1	2	7
10.222	1.94E5	1.70	1.06	6.15E-1	3.65E-1	1.39E-1	2	8
10.2179	1.81E5	1.37	1.06	4.71E-1	2.26E-1	6.32E-2	2	9
10.2141	1.79E5	1.03	1.05	3.16E-1	1.11E-1	2.17E-2	2	10
10.2107	2.16E5	.69	1.05	1.50E-1	3.48E-2	3.81E-3	2	11
10.2069	1.88E5	.43	1.05	4.76E-2	5.96E-3	3.89E-4	2	12

- LD-SCAN is a subroutine which scans the light diaphragm opening while the pressure remains at a fixed value, thus operating the counter similarly to a threshold one.

The display is the same as from the pressure scanning subroutine and it can be used to determine the maximum opening for the light diaphragm in order to avoid counting unwanted particles while allowing the best possible efficiency.

5. PRACTICAL OPERATION

When a new experiment is being set up, EA experts help to put the CEDAR(s) into operating condition, and at the same time instruct the users on how to do it themselves.

5.1 Particle separation and CEDAR resolution

The separation in millimetres of Čerenkov light rings at the light diaphragm is shown as a function of the beam momentum and for various particles in Figs. 20 and 21. In order

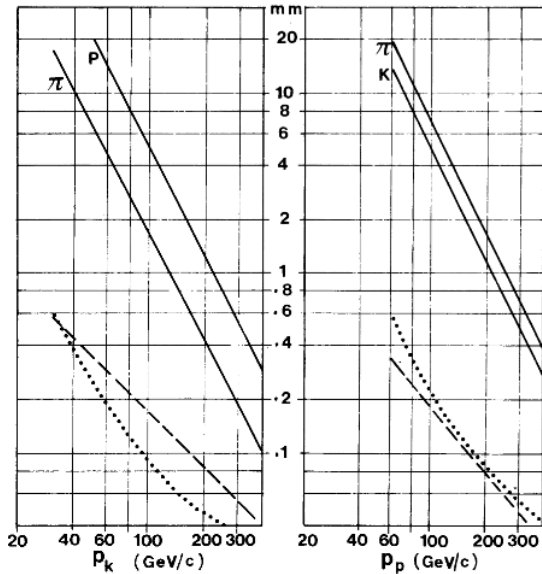
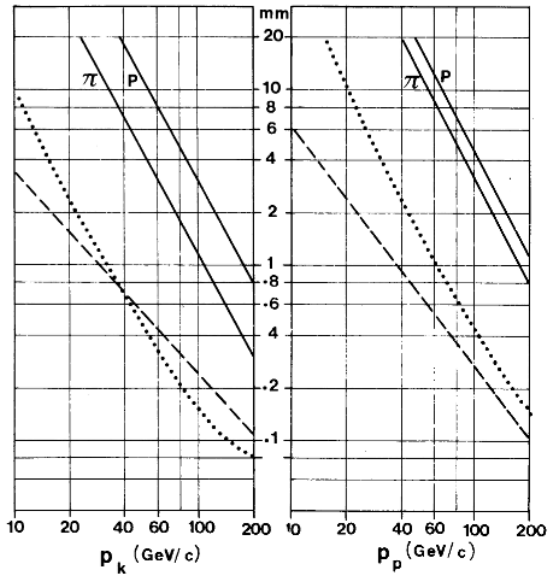
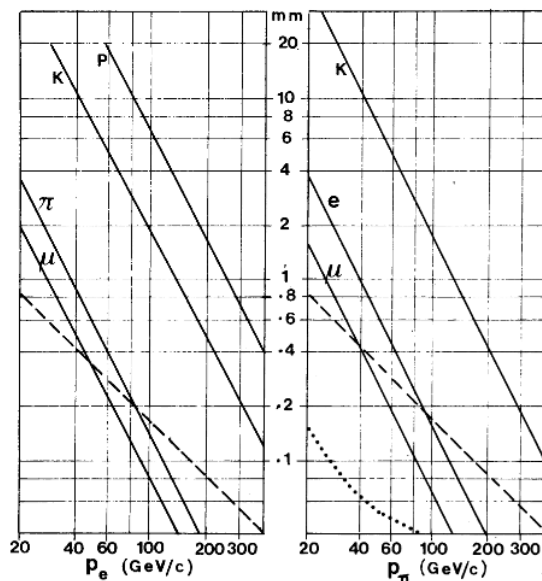
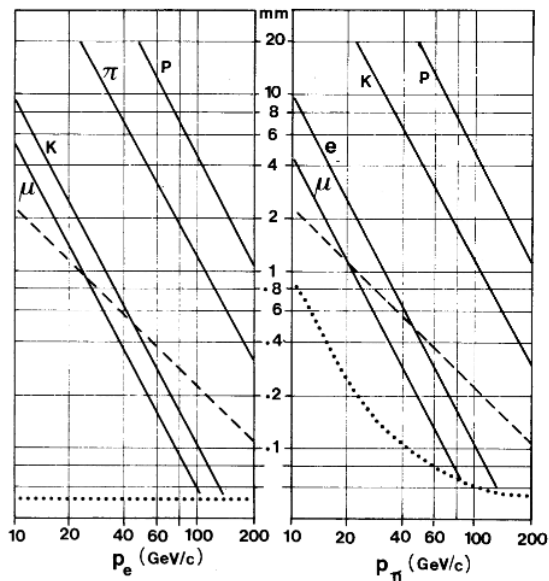


Fig. 20 CEDAR N

Fig. 21 CEDAR W

Radial distance in the plane of the diaphragm between the light rings of the wanted and of various unwanted particles versus beam momentum. The dotted line indicates the width of the light spot (4σ) and the dashed line gives the contribution to the light spot of the multiple scattering (4σ).

to get a good particle identification, this separation must be larger than the width of the light rings for which the two main contributions are also shown in Figs. 20 and 21.

Example: For a CEDAR-N set on kaons at 200 GeV/c, one reads from Fig. 21 a light spot of 46 μm , a multiple scattering effect of 85 μm , and a distance to the pion ring of 400 μm , so that an LD opening between 200 μm and 400 μm would be adequate.

Closing the light diaphragm gives a better rejection of the unwanted particles, but a worse efficiency of counting the good ones, especially in the presence of beam divergence.

5.2 Efficiency

Counting efficiencies depend upon various factors: status of optics and of photomultipliers, LD opening, gas pressure, beam momentum, angle of the particle trajectory (due to beam divergence and CEDAR alignment), and choice of the sixfold, sevenfold, or eightfold coincidence level. The counting efficiencies are related to the NPE seen by a photomultiplier by the expressions given in Appendix A and shown in Fig. 8. The sixfold coincidence reaches a high efficiency already with NPE = 2, whereas the eightfold one hardly goes beyond 60% for $\text{NPE} \leq 3$. Typical numbers of photoelectrons are between 2.5 and 3 for a CEDAR-N and between 3 and 3.5 for a CEDAR-W, with LD wide open. Past experience indicates that the sixfold level

Table 5
6-fold efficiency of CEDARs as measured in Ref. 10

Energy, polarity (GeV/c)	p_T (GeV/c)	CEDAR-1			CEDAR-2		
		LD (mm)	Efficiency (%)	Number of points	LD (mm)	Efficiency (%)	Number of points
-60	0	0.62	85.2 \pm 0.6	3	0.62	66.6 \pm 0.6	3
	0.5	2.52	96.6 \pm 0.3	3	2.52	93.7 \pm 0.15	3
+60	0	2.52	96.9 \pm 0.3	6	2.52	94.0 \pm 0.5	6
	0.5						
-120	0						
	0.3	1.24	95.7 \pm 0.18	9	1.24	92.5 \pm 0.23	9
	0.5						
+120	0						
	0.3	1.24	94.85 \pm 0.27	9	1.24	91.13 \pm 0.54	9
	0.5						
-200	0	0.23	80.0 \pm 1.8	3	0.23	69.5 \pm 1.5	3
	0.5	0.23	66.2 \pm 2.0	3	0.23	71.8 \pm 3.3	3
+200	0	0.31	86.71 \pm 1.3	3	0.25	78.34 \pm 0.5	3
	0.5				0.31	77.6 \pm 1.0	3
-300	0	0.13	58.2 \pm 0.3	3	0.13	50.6 \pm 0.4	3
	0.5	0.13	56.2 \pm 1.5	3	0.13	48.9 \pm 1.5	3
+300	0.5	0.13	64.5 \pm 1.0	3	0.13	56.5 \pm 0.5	3

has a rejection power good enough for practically all applications encountered so far (one exception is described in Section 5.6).

The average efficiency also drops when the beam divergence is larger than the angular acceptance of the counter, given by the LD setting divided by the focal length. At very high energy, where one might have to close the LD to 0.1 mm, the acceptance is $0.1 \text{ mm}/3.88 \text{ m} = 26 \mu\text{rad}$ for a CEDAR-N. Keeping a beam parallel to this level of precision requires a lot of attention. In the best case there will always be some tail in the divergence distribution for which the counting efficiency is lower.

As an indication of the efficiencies one can reach in practice, we give in Table 5 the measured absolute values obtained in an experiment with 400 GeV/c protons¹⁰). The H2 beam had been carefully optimized for those CEDAR measurements.

5.3 Procedure for the tuning and setting up of a CEDAR

- i) The parallelism of the beam must be tuned to provide a beam divergence smaller than the counter acceptance, see Section 5.2.
- ii) In order to ensure an easier operation of the trigger counters and of the CEDAR during the tuning, it is better to keep the beam intensity below, say, $10^6/\text{s}$ by collimating the beam size without altering the beam divergence at the CEDAR.
- iii) Print the STATUS of the CEDAR to check its current pressure, temperatures, etc., and to read the nominal values of pressure corresponding to the different particles. Then set the pressure for the most abundant particle (protons in a positive beam, pions in a negative one).
- iv) Open the diaphragm (LD = 20 mm), using the program ALIGN, to measure NPE and to check that all photomultipliers are efficient: the ratios of the photomultipliers counts to the triggers counts should not be less than 90% [if the beam energy is high enough so that all the light rings of π , K, and p are falling inside the diaphragm opening; this can be checked on Figs. 20 and 21]. The ratios of photomultiplier efficiencies right/left (R/L) and up/down (U/D) obtained with the open diaphragm are to be kept as reference.
- v) Align the CEDAR in the beam in order to optimize its performances (Fig. 4c). This is achieved by trying to reproduce the same values of R/L and U/D after a reduction of the diaphragm opening. It is preferable to reduce LD in steps, since the alignment gets more and more tricky with smaller diaphragms! The real optimum is reached when the values R/L and U/D are the same as for the wide open diaphragm [paragraph (iv) above] and NPE is simultaneously at a maximum. One should not worry if the efficiencies of the right and left photomultipliers (2, 3, 6, 7) are not the same as the efficiencies of the top and bottom ones (1, 4, 5, 8); this is generally the case because of different beam divergences in the horizontal and vertical planes. But, if the overall efficiency is well below what might be expected for the particle on which the alignment is done, something more fundamental should be checked, e.g. the pressure.
- vi) The nominal pressures given by the program might be slightly wrong because of a gas pollution by air or vessel outgassing. A pressure scan is the best way to check the correct pressure setting. This is a lengthy procedure if one intends to go through several particle peaks, because at low momentum the big change of pressure is time

consuming, and at high momentum the good resolution can only be achieved with a perfect thermal equilibrium in the gas radiator. When the vessel pressure is increased by a gas inlet there is an overall adiabatic temperature increase plus a local inlet of cool gas (expansion at the valve). The latter effect is dangerous because of the long time constant (about one hour) needed to reach thermal equilibrium, which is due to the length of the counter. But when a gas outlet is made, there is a uniform decrease of temperature followed by an equilibrium reached with a time constant of 15 s. Therefore, with $\Delta P = -3$ mbar between points, an accuracy of 1 mbar would be reached only if one waits 15 s before each measurement. A scan done at a higher speed will neither reach the ultimate resolution (best dip between peaks) nor give the pressure with an accuracy of 1 mbar.

In summary, a pressure scan should be done by decreasing the pressure, with an LD setting smaller than or equal to the distance from the nearest particle peak (see Figs. 20 and 21) and with a number of points large enough to get a small ΔP between two measured points. Points are currently measured every two cycles of the SPS with a time interval of typically 24 s.

As an example, Figs. 22 and 23 show a pressure scan around the π and K peaks, made with two different values of LD. Only the sixfold majority signal is plotted, since it is most in use, except for some special cases (see Section 5.6).

- vii) Fine tuning of the LD. If the particle separation is not sufficient, close the LD slightly and make another pressure scan. If instead it is more than sufficient, but for some reason -- especially large beam divergence at the CEDAR -- the efficiency is low, then an LD scan will prove useful to optimize the LD value. Set the pressure on the selected particle peak [measured as in paragraph (vi)] and then ask for an LD-SCAN

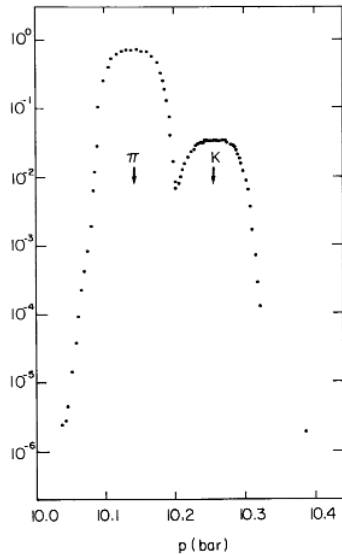


Fig. 22 LD = 0.50 mm

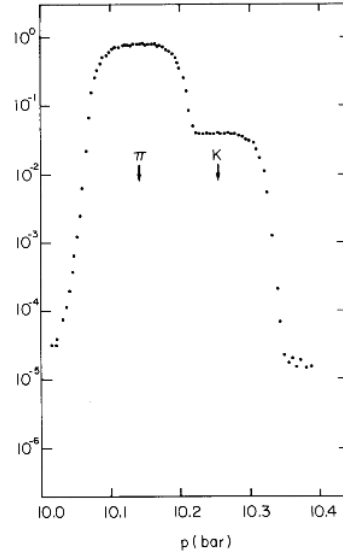


Fig. 23 LD = 0.71 mm

CEDAR-N pressure scan showing the π /K separation in the H6 beam running at -175 GeV/c.

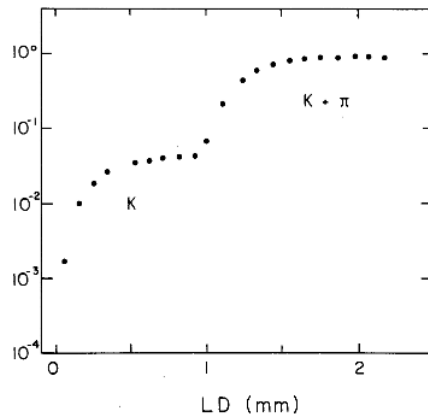


Fig. 24 LD scan with pressure set on the kaon mass.
CEDAR-N in beam H6 as for Figs. 22 and 23.

from say 0.05 mm to twice or three times the particle separation. The output, when conveniently plotted (see Fig. 24), will give a hint on efficiency and rejection of the CEDAR at the various LD settings. In fact, the wide LD setting of Fig. 23 has been decided after first doing the pressure scan with smaller LD, also shown in Fig. 22, and then the LD scan shown in Fig. 24. In this particular case the beam divergence was 50 μ rad FWHM in the vertical plane and 120 μ rad in the horizontal plane.

5.4 Monitoring the CEDAR stability

The monitoring of the index of refraction is a bit more delicate since it does not depend only upon pressure, but also upon temperature (in fact, upon P/T, see Section 3.3.1). The program MASS is meant to help there: during data taking, one should note the wanted mass and restore it by using the program if the value has shifted.

When operating at the utmost resolution, it is necessary to make a pressure scan to check the centre of the peak as indicated in Section 5.3, paragraph (vi). The gas pressure at the centre of the peak corresponds to a value of mass (read via the MASS or STATUS programs) slightly off the known particle mass, because the gas purity is never perfect. This fictitious mass value is to be kept during data taking.

5.5 Operation at high beam intensity

CEDARs set on minority particles have been operated satisfactorily in beams with total intensities exceeding 5×10^7 particles/s. As mentioned in Section 5.1, such intensities are often achieved by sacrificing somewhat the beam parallelism at the CEDAR so that the counting rate of the individual photomultipliers can be much larger than the rate of the wanted particles. Even under those conditions the photomultipliers do tolerate single counting rates of 10^7 counts/s. The efficiency depends strongly on the relative values of LD and beam divergence.

5.6 Selection of electrons and muons

Electrons and muons are often used for calibration purposes in hadron beams. A CEDAR-N can separate electrons from pions up to 60 GeV/c -- but then the use of the eightfold

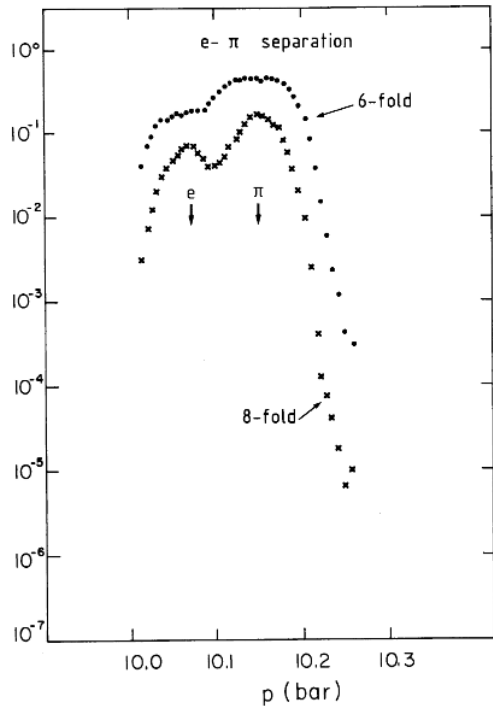


Fig. 25 Pressure scan for CEDAR-N showing the separation of electrons and pions at $-60 \text{ GeV}/c$

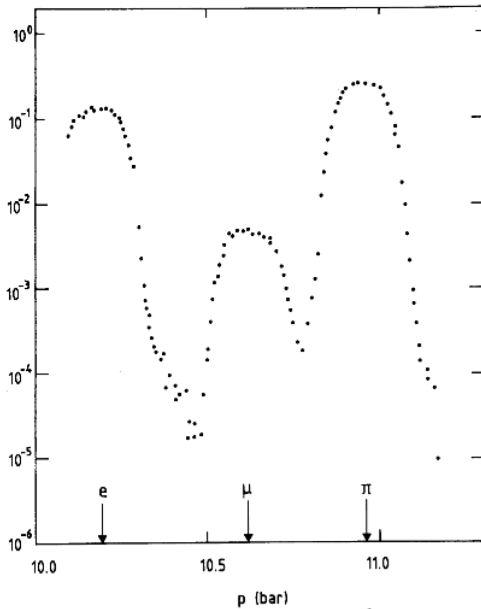


Fig. 26 Pressure scan for CEDAR-N showing the separation of electrons, muons, and pions at $20 \text{ GeV}/c$

coincidence is necessary, see Fig. 25. At lower energies, of course, the separation becomes easier; one may use the sixfold coincidence and also a CEDAR-W. Figures 20 and 21 will help in assessing the performance at a given energy. The same can be said for the separation of muons: Fig. 26 shows a CEDAR-N scan, in which electrons, muons, and pions are well separated in a $20 \text{ GeV}/c$ beam.

Acknowledgements

It is a pleasure to express our appreciation to S. Milner for leading the mechanical design effort at the beginning of the CEDAR project and to M. Rabany and members of his group for their design of the electronics and the subsequent care they took in its implementation and operation. The meticulous assembly of the light diaphragm was carried out by J. Stirnimann and that of the xy tables and gas-handling system by J.L. Loquet. The refractometer used for the laboratory calibration of the refractive index was designed by M. Benot and the associated electronics was built by Y. Bernard. E. Rossa participated in the first tests of the optical system and, with the help of G.P. Ferri, has been responsible for the functioning of the CEDARs since 1980. R. Saban helped to provide adequate software, and improvements to the package described in Section 4 are due to the initiative of M. Glaser. In addition, we are grateful to all our EA colleagues, who have worked with great competence to develop the use of CEDARs. Among the many experimental teams who have made use of the counters we particularly wish to acknowledge the participation of T. Ekelöf in the early stages of operation, and the interest shown by members of experiment NA3 in exploiting CEDARs at high particle fluxes.

REFERENCES

- 1) M. Benot, J. Litt and R. Meunier, Čerenkov counters for particle identification at high energies, Nucl. Instrum. Methods 105, 431-444 (1972).
- 2) C. Bovet, S. Milner and A. Placci, Internal Report CERN/Lab. II/EA/74-4 (1974).
- 3) C. Bovet, R. Maleyran, A. Placci and M. Placidi, The CEDAR (Čerenkov differential counters with achromatic ring focus) project, IEEE Trans. Nucl. Sci. NS25, 572 (1978).
- 4) V.P. Zrelov, Čerenkov radiation in high-energy physics (Atomizdat, Moscow, 1968), translated from Russian by Israel Programme for Scientific Translations, Jerusalem, 1970, vols. I and II.
- 5) R.P. Feynman, R.B. Leighton and M. Sands, The Feynman Lectures on Physics (Addison-Wesley, Reading, Mass., 1964), vol. II, Eq. (32.7).
- 6) The Hamilton standard model 1D digital pressure transducer, Instruction Manual.
- 7) M. Placidi, SPS/EA/Note 76-20 and SPS/EA/Note 76-21 (1976).
- 8) P. Dreesen, SPS/EBS/Note 78-15 (Rev. 2.4.1979).
- 9) C. Bovet, A. Placci and M. Placidi, Paper in preparation.
- 10) H.W. Atherton, C. Bovet, N. Doble, G. von Holtey, L. Piemontese, A. Placci, M. Placidi, D.E. Plane, M. Reinharz and E. Rossa, Precise measurements of particle production by 400 GeV/c protons on beryllium targets, CERN 80-07 (1980).

APPENDIX A

STATISTICS OF PATTERN RECOGNITION

Assuming that the number of photoelectrons detected by a photomultiplier follows a Poisson distribution, the probability of missing an event is

$$P_\phi(0) = e^{-\phi} , \quad (A.1)$$

where ϕ is the average number of photoelectrons and

$$P_\phi(k) = \frac{e^{-\phi} \phi^k}{k!} \quad (A.2)$$

is the general term of the distribution. Of course, the efficiency η of one photomultiplier which detects on an average ϕ photoelectrons is

$$\eta = 1 - P_\phi(0) = 1 - e^{-\phi} . \quad (A.3)$$

When eight photomultipliers are looking at the same event with equal efficiencies η and equal chance of not seeing it, $\varepsilon = 1 - \eta$, then the probabilities of various levels of coincidence can be seen from the binomial expansion:

$$(\eta + \varepsilon)^8 = \eta^8 + 8\eta^7\varepsilon + 28\eta^6\varepsilon^2 + 56\eta^5\varepsilon^3 + 70\eta^4\varepsilon^4 + 56\eta^3\varepsilon^5 + 28\eta^2\varepsilon^6 + 8\eta\varepsilon^7 + \varepsilon^8 . \quad (A.4)$$

The first term on the right-hand side of Eq. (A.4) is the probability of the eight photomultipliers flashing (eight coincidence level), the next term is for seven and only seven, the next term is the probability of six and only six photomultipliers flashing, etc. So that one can write the following probabilities for different majority levels:

$$\begin{aligned} \eta_8 &= \eta^8 \\ \eta_7 &= \eta_8 + 8\eta^7\varepsilon \\ \eta_6 &= \eta_7 + 28\eta^6\varepsilon^2 \\ &\dots \end{aligned} \quad (A.5)$$

From the measured values of these coincidence levels one can deduce the average number of photoelectrons ϕ for the wanted particles as follows:

$$\frac{\eta_7}{\eta_8} = 1 + 8I , \quad (A.6)$$

where $I = e^{-\phi}/(1 - e^{-\phi})$, and conversely

$$\phi = \ln(1 + I) - \ln I . \quad (A.7)$$

And from Eqs. (A.6) and (A.7) one has

$$\phi = \ln \left[1 + \frac{8}{\eta_7/\eta_8 - 1} \right] . \quad (A.8)$$

Similarly with η_6 one can write

$$\frac{\eta_6}{\eta_8} = 1 + 8I + 28I^2 , \quad (A.9)$$

and solving for I gives

$$I = \frac{-2 + \sqrt{4 - 7(1 - n_6/n_8)}}{14}, \quad (\text{A.10})$$

and finally, using Eq. (A.7) one gets

$$\phi = \ln \left[1 + \frac{14}{\sqrt{4 - 7(1 - n_6/n_8)} - 2} \right]. \quad (\text{A.11})$$

The two values given by Eqs. (A.8) and (A.11) are used for a consistency check.

APPENDIX B

ALGORITHM FOR COMPUTER CONTROL OF THE INDEX OF REFRACTION

The following symbols are used:

- ρ , P , T = density (g/cm^3), pressure (bar), absolute temperature (K), of the gas, respectively.
 p , m = momentum (GeV/c) and rest mass (GeV) of detected particle, respectively.
 a = gas constant (cm^3/g) for a given light wavelength.
 $k(\lambda)$ = gas constant (K/bar) for a given light wavelength.
 θ = Čerenkov angle.
 n = index of refraction of CEDAR radiator.

1. BASIC RELATIONS

From the definition of Čerenkov angle, the refractive index is

$$n = \frac{1}{\beta \cos \theta} = \frac{\sqrt{1 + (m/p)^2}}{\cos \theta} \quad (\text{B.1})$$

and assuming a linear dependence of n on gas density we have

$$n - 1 = ap = k \frac{P}{T} \quad (\text{B.2})$$

Given the angle θ^* defined by the optics of the instrument we can derive from Eqs. (B.1) and (B.2) the gas pressure needed to detect a particle of mass m and momentum p

$$P = \frac{T}{k} \left[-1 + \frac{\sqrt{1 + (m/p)^2}}{\cos \theta^*} \right]. \quad (\text{B.3})$$

Conversely, for any set of values of p , T , and P we can compute a mass m which satisfies the relation

$$m = p \sqrt{-1 + \cos^2 \theta^* \left(1 + k \frac{P}{T} \right)^2}. \quad (\text{B.4})$$

From Eq. (B.3) a lower limit for gas pressure is defined by the condition of having Čerenkov light produced at angles $\theta \geq \theta^*$

$$P_{\min} = \frac{T}{k} (n - 1)_{\min}, \quad (\text{B.5})$$

where

$$(n - 1)_{\min} = \frac{1}{\cos \theta^*} - 1 \quad (\text{B.6})$$

is the minimum value ($\rho = \infty$) for the gas refractive index.

The relations (B.3), (B.4), and (B.5) are evaluated in the CEDAR control programs, taking into account the actual average gas temperature T .

2. LIMITS ON MASS DEFINITION FROM MEASUREMENT ERRORS ON P AND T

From Eq. (B.4):

$$\Delta m = \Delta P^* \left(\frac{\partial m}{\partial P} \right) + \Delta T^* \left(\frac{\partial m}{\partial T} \right),$$

where ΔP^* and ΔT^* are the measurement errors on the gas parameters P and T.

Derivation of Eq. (B.4) gives

$$\frac{\partial m}{\partial T} = -\frac{P}{T} \left(\frac{\partial m}{\partial P} \right)$$

$$\frac{\partial m}{\partial P} = \frac{k \cos \theta^*}{T} \left(\frac{p^2}{m} \right) \sqrt{1 + \left(\frac{m}{p} \right)^2} \approx \frac{k \cos \theta^*}{T} \left(\frac{p^2}{m} \right). \quad (B.7)$$

The mass uncertainty is then

$$\Delta m \approx \frac{kP}{T} \frac{p^2}{m} \cos \theta^* \left(\frac{\Delta P^*}{P} + \frac{\Delta T^*}{T} \right). \quad (B.8)$$

3. SUMMARY OF PARAMETER VALUES

Some numerical evaluations of the above-defined quantities are collected in the following table, assuming

$$T = 293.16 \text{ K } (20^\circ \text{C})$$

$$\lambda = 300 \text{ nm}.$$

CEDAR type	W	N
gas	N_2	He
$k^a)$ (K/bar)	8.44665×10^{-2}	9.59168×10^{-3}
θ (mrad)	30.9	25.8
P_{\min} (bar)	1.647	10.175
P_{\max} (bar)	8	15
$(n - 1)_{\min}$	4.745×10^{-4}	3.329×10^{-4}
$\Delta P^b)$ (mbar)	1.6	3
$\Delta T^b)$ (K)	0.3	0.1
$\Delta P^{*c)}$ (mbar)	± 0.5	± 1
$\Delta T^{*c)}$ (K)	± 0.02	± 0.02
$\left(\Delta P^* + P_{\max} \frac{\Delta T^*}{T} \right)_{\max}$ (mbar)	$\leq \pm 1$	$\leq \pm 2$

a) Ref. 7.

b) As from Table 4. Requested accuracies.

c) Instrumental errors.

GENERAL MECHANICAL DRAWING

